


國立交通大學
光電工程研究所
碩士論文

聚乙烯醇包覆水溶性硒化鎘奈米粒子之非
線性光學及螢光光譜研究



Optical Nonlinearity and
Photoluminescence of PVA-capped CdSe
Nanoparticles

研究生：沈哲佑

指導教授：安惠榮 教授

中華民國九十九年八月

聚乙烯醇包覆水溶性硒化鎘奈米粒子之非線性光學
及螢光光譜研究

Optical Nonlinearity and Photoluminescence of PVA-capped
CdSe Nanoparticles

研究生：沈哲佑

Student : Che-Yu Shen

指導教授：安惠榮 教授

Advisor : Prof.Hyeyoung Ahn

國立交通大學

光電工程研究所

碩士論文

A Thesis

Submitted to Department of Photonics and

Institute of Electro-Optical Engineering

College of Electrical Engineering

National Chiao Tung University

In partial Fulfillment of the Requirements

for the Degree of

Master of Science

in

Electro-Optical Engineering

August 2010

Hsinchu, Taiwan, Republic of China

中華民國九十九年八月

Optical Nonlinearity and Photoluminescence of PVA-capped CdSe Nanoparticles

Student : Che-Yu Shen

Advisors : Prof. Hyeyoung Ahn

Department of Photonics and Institute of Electro-Optical Engineering

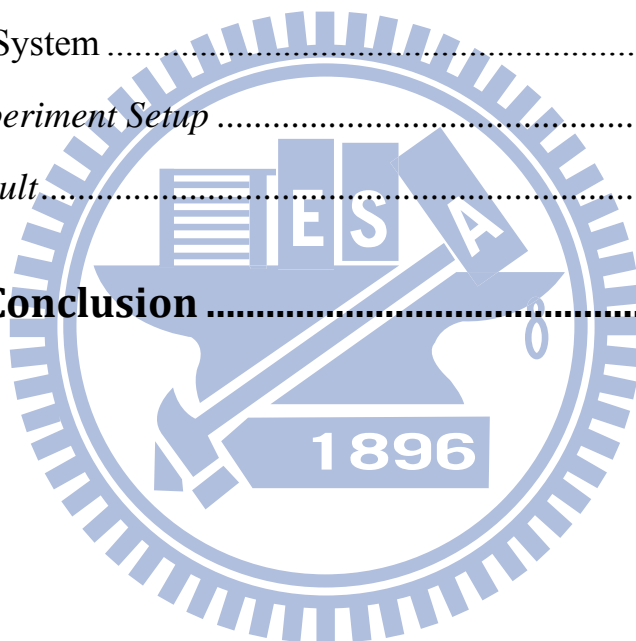
Abstract

In this thesis, we report the photoluminescence and optical nonlinearity of water-soluble PVA-capped CdSe nanoparticles with high quantum yield (around 68%). Luminescence properties of water-soluble CdSe nanoparticles were studied using time-integrated and time-resolved photoluminescence (TRPL) measurements at room temperature. We observed the photoactivation of CdSe nanoparticles induced by ultrafast laser pulses. By using the Z-scan measurement technique, we measured two photon absorption coefficient β of water-soluble CdSe nanoparticles.

Content

Chapter1	Introduction.....	1
1.1	Nanoparticles.....	1
1.1.1	<i>Surface Effect</i>	3
1.1.2	<i>Quantum Confinement Effect</i>	3
1.1.3	<i>Size Quantization Effect</i>	5
1.2	CdSe.....	6
1.2.1	<i>Chemical Colloidal Method</i>	7
1.2.2	<i>Core/Shell Structure</i>	8
1.2.3	<i>Hydrophilic Ligand</i>	10
1.2.4	<i>Applications of CdSe nanoparticle</i>	11
1.3	Motivation.....	11
Chapter2	Principles.....	13
2.1	Photoluminescence System.....	13
2.1.1	<i>Photoluminescence System</i>	13
2.1.2	<i>Time-resolved Photoluminescence System</i>	16
2.2	Z-scan System.....	18
2.2.1	<i>Basic Principle of Z-scan</i>	18
2.2.2	<i>Effects of Nonlinear Absorption</i>	25
Chapter3	Sample Preparation.....	27
3.1	Preparation of the CdSe Nanoparticle.....	27

3.1.1	<i>Materials</i>	27
3.1.2	<i>Procedure</i>	28
3.2	List of Samples.....	30
Chapter4	Experiment & Result	31
4.1	Photoluminescence and Time-resolved Photoluminescence System	31
4.1.1	<i>Experiment Setup</i>	31
4.1.2	<i>Result</i>	33
4.2	Z-scan System	52
4.2.1	<i>Experiment Setup</i>	52
4.2.2	<i>Result</i>	55
Chapter5	Conclusion	62



List of figures

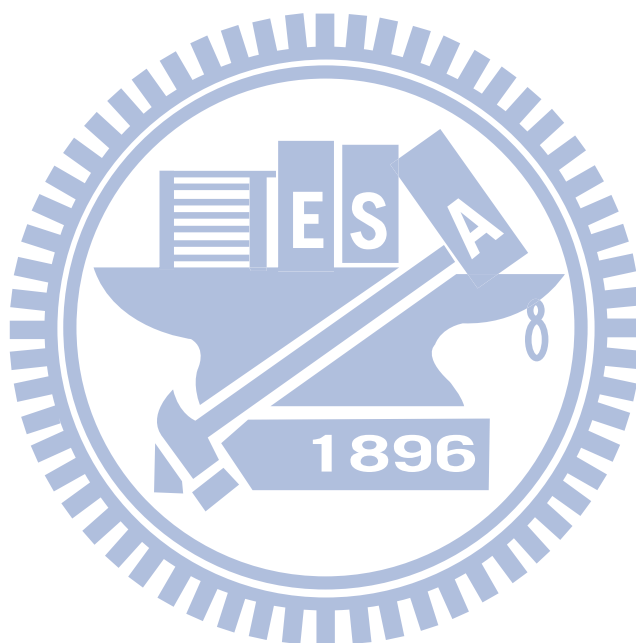
Fig. 1-1	The scale of things.....	1
Fig. 1-2	Fractions of atoms on the nanocrystal surface are plotted against the total number of atoms	2
Fig. 1-3	Molecular orbital model for different particle size.	4
Fig. 1-4	Characteristics of different colors of CdSe quantum dots	5
Fig. 1-5	Important discoveries over the years.....	7
Fig. 1-6	(A) Type-I core/shell structure (B) Type-II core/shell structure	9
Fig. 2-1	(1) Excitation. (2) Thermal equilibrium. (3) Recombination.....	14
Fig. 2-2	Radiative recombination paths: (a) band-to-band; (b) donor to valence band; (c) conduction band to acceptor.	15
Fig. 2-3	A typical photoluminescence spectrum.....	15
Fig. 2-4	The basic principle of time-resolved photoluminescence.....	17
Fig. 2-5	Basic experimental setup of Z-scan.....	18
Fig. 2-6	If n_2 is positive, when we move the sample, will get different power of laser beam.....	20
Fig. 2-7	If n_2 is negative, the laser beam diverges.	20
Fig. 2-8	The Z-scan data of transmittance change with Z/Z_0	21
Fig. 3-1	(a) Se precursor (b) Se precursor.....	29
Fig. 4-1	Photoluminescence and time-resolved photoluminescence system...	31
Fig. 4-2	Normalized PL intensity of sample C , D , J.....	33
Fig. 4-3	PL spectrum of sample C with different excitation times.....	34
Fig. 4-4	PL spectrum of sample J with different excitation times.....	35
Fig. 4-5	Schematic picture of the mechanism of the photoactivation reaction occurring on water-soluble CdSe nanoparticles and changes on PL intensity	

observed during this pathway.....	36
Fig. 4-6 Total PL intensity change with excitation time of sample E.....	38
Fig. 4-7 Total PL intensity change with excitation time of sample F.	38
Fig. 4-8 Total PL intensity change with excitation time of sample G.	39
Fig. 4-9 Total PL intensity change with excitation time of sample H.	39
Fig. 4-10 Modified photoactivation reaction.	41
Fig. 4-11 PL spectrum in different excitation times of sample E.	43
Fig. 4-12 PL spectrum in different excitation times of sample F.....	43
Fig. 4-13 PL spectrum in different excitation times of sample G.....	44
Fig. 4-14 PL spectrum in different excitation times of sample H.....	45
Fig. 4-15 Time-resolved photoluminescence curve of sample G,H.	47
Fig. 4-16 Total PL intensity change with excitation time of sample G at 400 nm.....	49
Fig. 4-17 Total PL intensity change with excitation time of sample H at 400 nm.....	49
Fig. 4-18 Time-resolved photoluminescence curve of sample G,H.	50
Fig. 4-19 Z-scan system setup.....	52
Fig. 4-20 Glass cell.....	53
Fig. 4-21 Normalized transmittance with S=1 of ZnTe.	54
Fig. 4-22 Normalized transmittance with S=1 of sample A.....	55
Fig. 4-23 Normalized transmittance with S=1 of sample B.....	55
Fig. 4-24 Normalized transmittance with S=1 of sample F.	56
Fig. 4-25 Normalized transmittance with S=1 of sample I.....	56
Fig. 4-26 Absorption of each samples.	58
Fig. 4-27 Different electric charges in Tris and PBS.	59

Fig. 4-28 The CdSe nanoparticles/PVA cluster..... 60

Fig. 4-29 FESEM imaging of sample F 60

Fig. 4-30 FESEM imaging of sample I 61



Chapter 1 Introduction

1.1 Nanoparticles

In recent years, nanotechnology becomes more and more important in many aspects of science. With the quick improvement of the colloidal science and nanoparticle inspection technology, nanoparticles, whether in basic scientific researches or advanced technology applications are subject to considerable attention and their applications have made great progress.

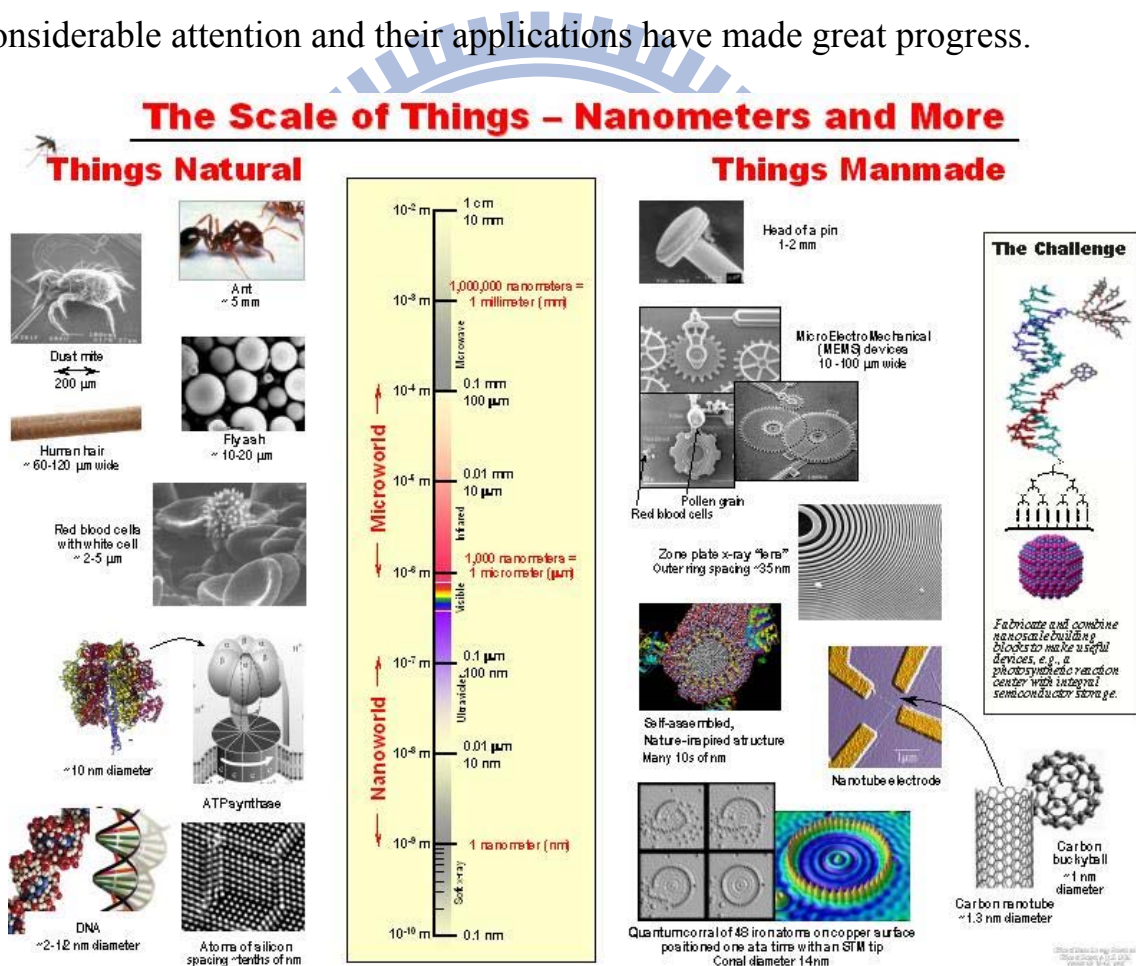


Fig. 1-1 The scale of things

[<http://cohesion.rice.edu/centersandinst/cnst/nano.cfm>]

In nanotechnology, a nanoparticle is defined as a small object that sizes between 1 and 100 nanometers ($\text{nm}=10^{-9} \text{ m}$)^[1]. In general, the nanoparticles consist of about ten to one million atoms. As the size become small, the fraction of atoms on surface becomes large. (see Fig.1-2) These nanoparticles bridge the gap between small molecules and large crystals, as well as enable the exploitation of the useful properties of materials.

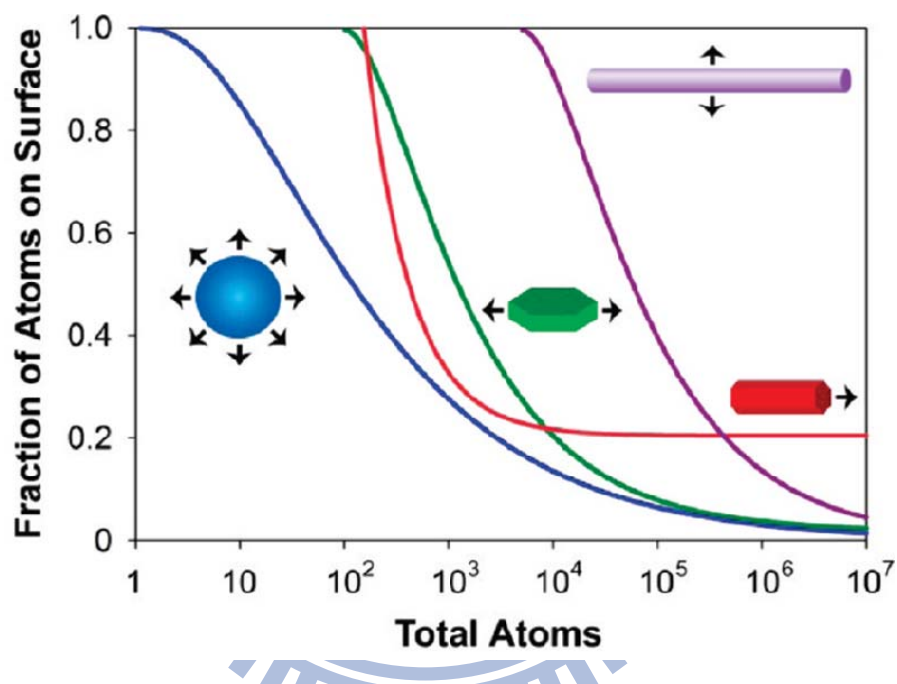


Fig. 1-2 Fractions of atoms on the nanocrystal surface are plotted against the total number of atoms^[1].

Recent study on nanoparticles found that material properties of substances in such a small scale appear different from those of the bulk, thus allowing the material to have many new applications. When the size is confined in this small range, three different effects have been found to occur, (1) surface effect^[1] (2) quantum confinement effect^[1], and (3) size quantization effect^[2].

1.1.1 Surface Effect^[1]

The surface effect means that as the crystal becomes smaller, the number of atoms on the surface increases, which can also impact the optical properties. Compare to bulk, the ratio of surface area and volume of nanoparticles is large, which allows a high surface energy. Because of the increase in the number of surface atoms, incomplete bonds within the crystal lattice and dangling bonds increase so that the surface atoms become unstable, highly reactive, and easily react with other atoms. The impact of the surface effect includes the nature of adsorption, catalytic and chemical properties, melting point and sintering temperature and changes in the mechanical properties of materials. For these reasons, the surface defects of nanoparticles with high surface-to-volume ratio strongly affect the optical properties of nanoparticles, such as the carrier relaxation and recombination sites. It will directly affect the luminescence properties of nanoparticles, and cause nonlinear optical effects. Therefore, if the surface quality of nanoparticles is improved, the quantum efficiency would be effectively improved.

1.1.2 Quantum Confinement Effect^[1]

In the macro view of the semiconductor materials, the space of exciton movement is not confined, so that the electron-hole pair separation is easy, and nonradiative relaxation would occur in the lattice defect. If the particle size is less than the Bohr radius (a_B), the exciton movement is limited in the small range and their average free path becomes short. In this case, the electron-hole pairs generate recombination emission easily and nanoparticles show some

special properties, of which their optical and electronic properties are dependent on the nanoparticle size.

$$E_n = \frac{n^2 h^2}{8m_{\text{eff}} a^2} \quad \text{Eq. 1-1}$$

$$\Delta E \propto \frac{1}{a^2} \quad a = \text{diameter} \quad \text{Eq. 1-2}^{[3]}$$

According to Eq. 1-2, as the particle size decreases, the quantum confinement effect increases and the energy gap moves to a higher energy, resulting the blue shift. On the bulk materials, since the number of atoms is large, the energy level spacing is very small and density of states is large. Therefore, it can be considered as a continuous energy band. However, for materials with the particle size in the nanometer scale, due to the reduction of the number of atoms, density of states is reduced and energy level spacing increases, and then it is no longer a continuous band, but non-continuous energy levels. Fig. 1-3 shows the molecular orbital energy level corresponding to different size of particles. This is called quantum confinement effect.

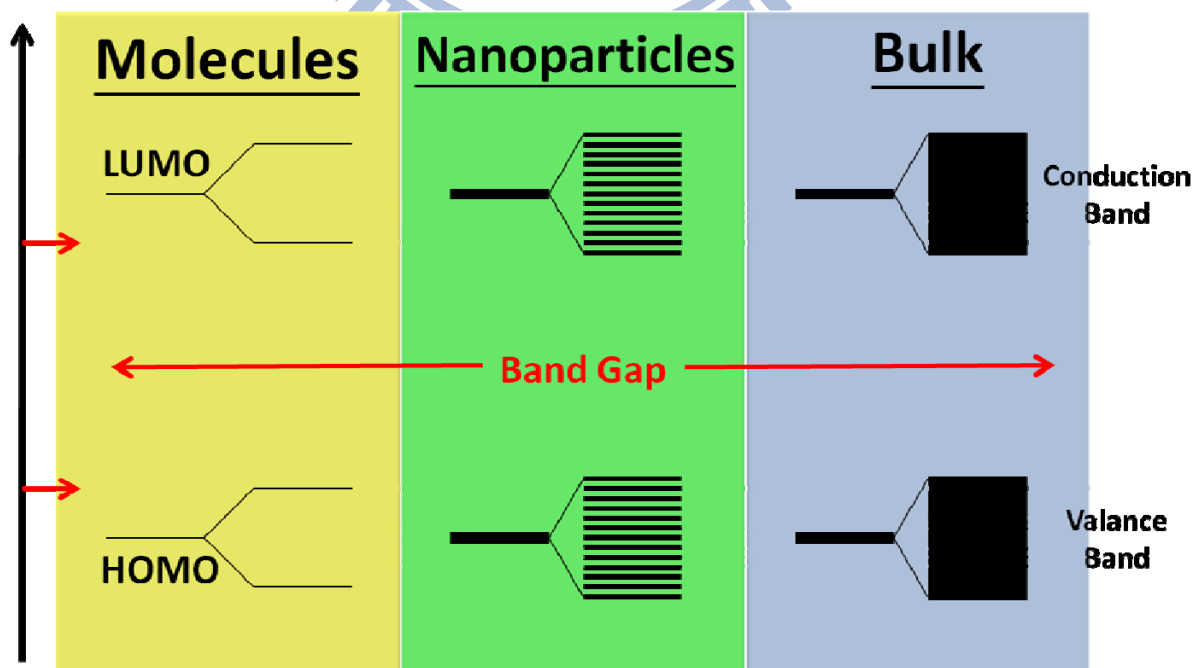


Fig. 1-3 Molecular orbital model for different particle size.^[3,4]

1.1.3 Size Quantization Effect^[2]

By controlling the shape, size, and structure of nanostructures, one can easily control the band gap, exciton binding energy, and so on. With the decrease of size of nanostructures, the UV-Visible absorption spectrum peak moves to the short wave length, and this blue shift corresponds to the size quantization effect. For example, the energy gap of cadmium selenide (CdSe) semiconductor bulk material is about 1.74 eV, while that of CdSe semiconductor quantum dots with the average diameter of 4.4 nm is 2.40 eV.^[5]

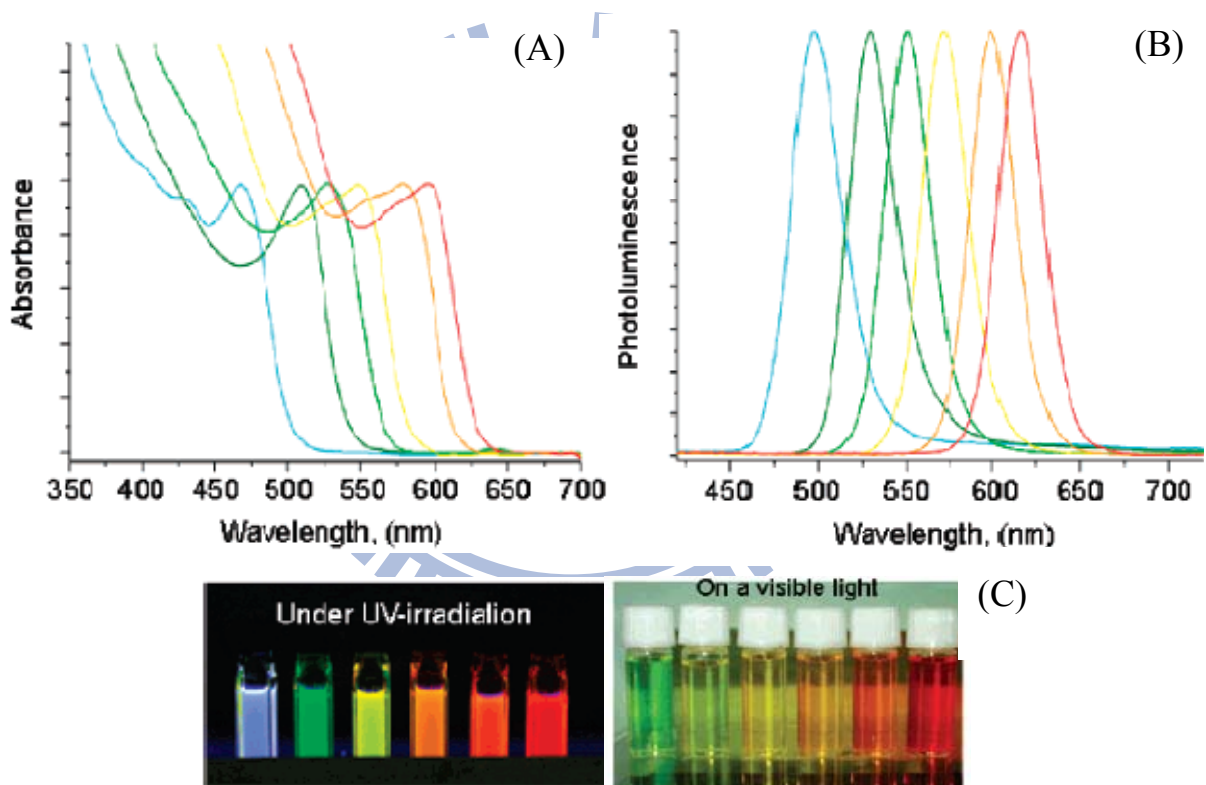


Fig. 1-4 Characteristics of different colors of CdSe quantum dots

(A) normalized absorbance spectra; (B) normalized PL spectra

($\lambda_{\text{ex}}=420\text{nm}$) ; (C) images under UV irradiation and on visible light.^[2]

1.2 CdSe

The traditional semiconductor device manufacturing way is top-down process by using etching techniques for miniaturization of material. With the improvement of technology, component size is possible to reach sub-micron, but if it is decreased further to the nanometer range, manufacturing process will face very harsh conditions and cannot be achieved easily by the present technology. And recently, bottom-up process based on atoms or molecules have been gradually raised.

In recent years, semiconductor nanomaterials researches are already mature in basic principles, preparation or applications and in particular CdSe semiconductor nanoparticles are well exploited^[6,7,8].

According to the section described above, nanoparticles have a high surface area/volume ratio so that surface defect strongly influences the optical properties of nanoparticles. By using a larger gap of the organic ligand coating on the surface of the nanoparticles^[8,9,10], or inorganic material attached^[11,12,13], we can form a core-shell structure. It can be used to enhance stability against chemical degradation, and thus reduce the electron hole pair non-radiative recombination with the surface defects as well as reduce the nanoparticles aggregation. Most importantly, it can increase the quantum yield. In the following, we will introduce the evolution of CdSe nanoparticles and the core-shell structure synthesis technology.

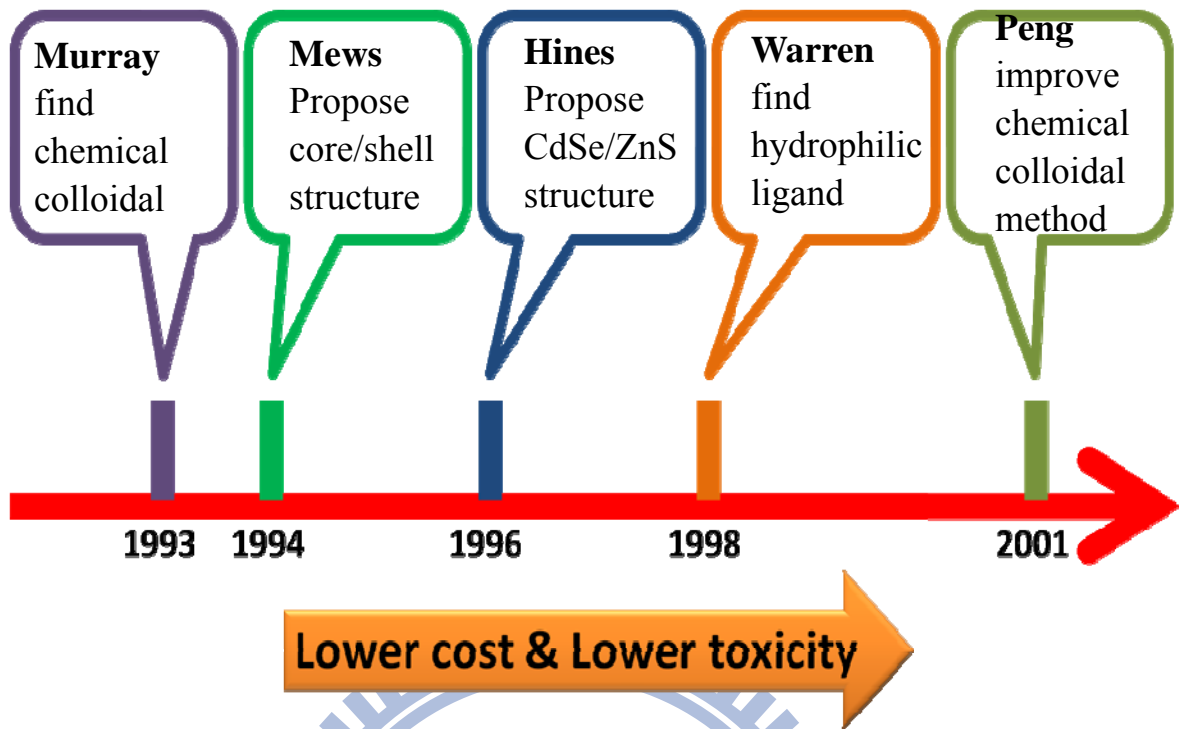


Fig. 1-5 Important discoveries over the years.^[6,14,15,16,17]

1.2.1 Chemical Colloidal Method

In 1993, from the Massachusetts Institute of Technology Murray's team first use of “**Chemical Colloidal Method**” in the organic phase synthesis of II-VI semiconductor quantum dots.^[6] The dimethylcadmium (CdMe_2) as cadmium precursor, produces a single size distribution and high crystallinity of CdSe quantum dots. Compared to earlier “**Lithography and Etching Processes**”^[18], Murray proposed a method which has a good reproducibility, and the ability to prepare quantum dots out of uniform size distribution. Since the particle size can be regulated by the reaction time in this method, spectra show a narrow absorption peak as well as band-edge emission peak. Following this success, most of synthesis of nanoparticles is practiced by using chemical colloidal method. However, CdMe_2 is toxic and explosive. Despite the use of a strong coordination ability of TOP (trioctylphosphine), TOPO (trioctylphosphine

oxide), protection agents and solvent also have the cost and toxic problems. In addition, the reaction temperature up to 250 ~ 300 degrees also limits the further application.

In 2001, an improved method was proposed by Peng et al. ^[17] of which a relatively low toxicity and stable CdO, Cd(AcO)₂ and CdCO₃ successfully used to synthesize CdSe, CdS, CdTe quantum dots with high crystalline quality quantum dots and low cost.

1.2.2 Core/Shell Structure

In 1994, Mews et al. proposed a method to produce "core-shell structure" of the quantum dots by chemical colloidal method, in which a layer of organic (or inorganic) compounds (such as zinc sulphide, zinc selenide, etc.) is added to the surface of quantum dots. This method limits the energy of excitation and then reduces non-radiative energy loss and increase photochemical stability. On the other hand, this method can reduce the lattice mismatch, and increase the efficiency of quantum dot emission.

In 1996, Hines used CdSe quantum dots as the core with the outer nuclear layer of ZnS to form a core/shell structure of the quantum dots. Compared to original CdSe quantum dots, the quantum efficiency of CdSe/ZnS quantum dots was increased by 6 times. The red-shift of photoluminescence spectroscopy peak of CdSe/ZnS quantum dots confirms the formation of core-shell structure.

Core-shell structure can be divided into Type-I^[15,19,20] and Type-II^[21] quantum dots according to the energy levels. (see Fig. 1-6) CdSe/CdS, CdSe/ZnS, CdSe/ZnSe, CdS/ZnS, ZnSe/ZnS belong to Type I. For Type I quantum dots, the shell energy gap is larger than the core energy gap. The shell conduction band is

higher than that of the core, but the shell valence band is lower than that of nuclear. On the other hand, for type-II including CdTe/CdSe, CdTe/CdSe, CdSe/ZnTe, ZnTe/CdSe, the conduction band and valence band of the shell is higher or lower than those of core.

Therefore, for Type-I quantum dots, the electron and hole are confined to the core and they have higher probability of recombination and reduced fluorescence lifetime, and consequently higher luminous efficiency; but the Type- II quantum dots have the completely opposite characteristics.

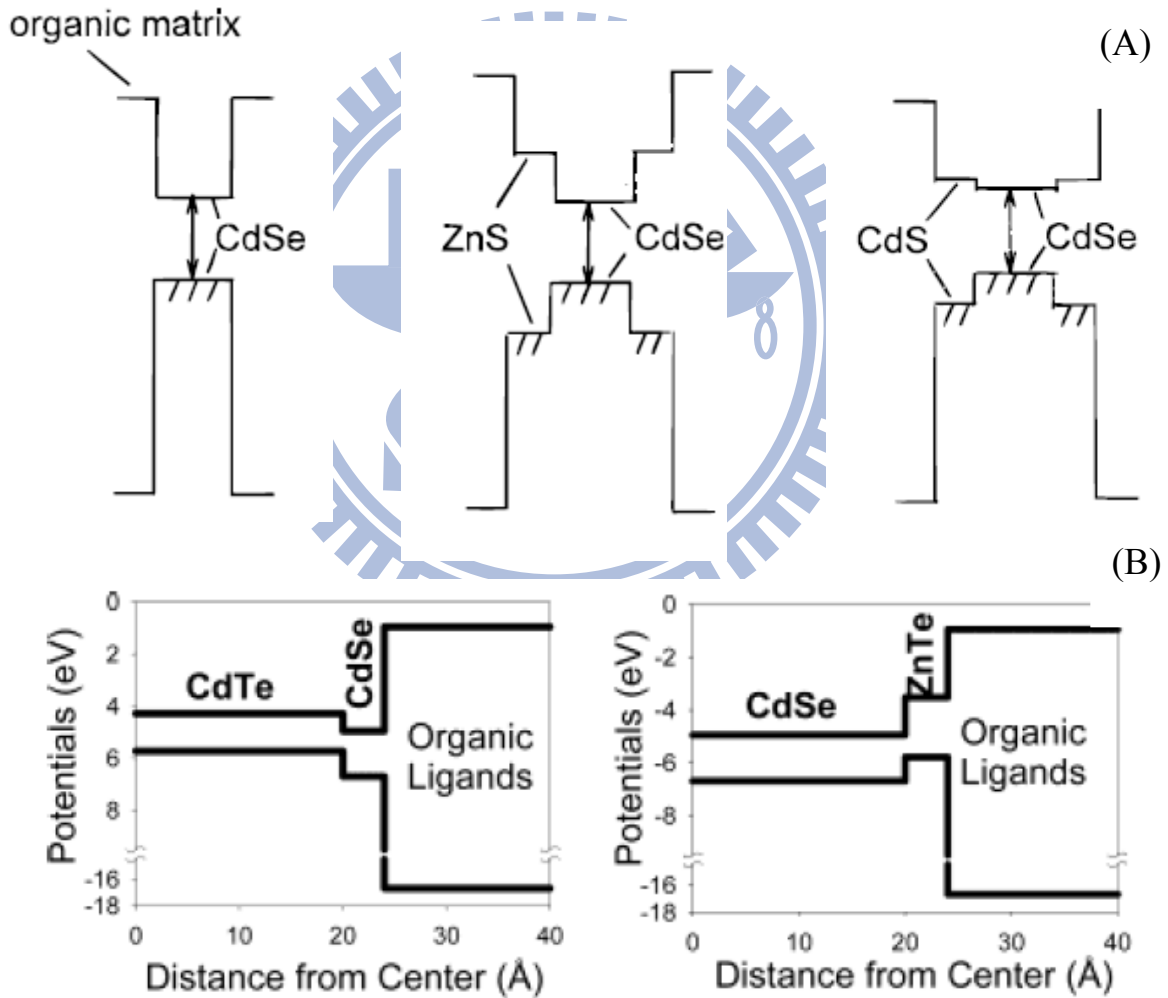


Fig. 1-6 (A) Type-I core/shell structure (B) Type-II core/shell structure

1.2.3 Hydrophilic Ligand

Even though the synthesis method of quantum dots in organic solvents has been developed quite completely, the reaction in toxic solvents and risk of pollution remain the most serious problems. So far, we have described that nanoparticles or core/shell structure by the traditional method are not soluble in water, indicating hydrophobic. Therefore, they are incompatible with the organism and their applications are quite limited. The search for the method to synthesize low toxicity, safe and water-soluble CdSe nanoparticles were gradually merged to change the quantum dot surface for hydrophilic modification or replacement. Goal is to synthesize low toxicity, safe and water-soluble CdSe nanoparticles.

In 1998, Nie and Chan proposed a method to modify CdSe / ZnS quantum dot surface by using mercaptoacetic acid and solved the problem of the water solubility and protein binding.^[16] Zinc atoms of CdSe / ZnS outer layer bonding with the mercapto group let a polar-COOH coat the most outer layer and make CdSe / ZnS quantum dots soluble in water.

While the above method can convert quantum dots from organic phase to the aqueous phase, the process of replacement of functional groups will produce a lot of defect to cause fluorescence quench and cause nanoparticles to fuse together, which makes the quantum dot fluorescence decay extremely fast and initiates precipitate formation and lowering of the quantum yield.

Therefore, it is crucial to directly synthesize high-quantum-yield water-soluble quantum dots in biomedical or optoelectronic applications.

1.2.4 Applications of CdSe nanoparticle

Compared to the general common fluorescent dyes, quantum dots have strong light stability and different particle size QD can emit different wavelengths of light with narrow spectral width and high output power. These unique optical properties cause a lot of attention in the quantum dots solar cells^[22,23,24], quantum dots light emitting diodes^[25,26], quantum dots biomedical sensors^[27,28], etc.

1.3 Motivation

Today, most of the high-quality CdSe nanoparticles were prepared by the pyrolysis of unsafe organometallic reagents in high-temperature organic solvents such as tri-n-octylphosphine/tri-n-octylphosphine oxide (TOP / TOPO). But this approach is neither suitable for large-scale synthesis nor environment-friendly. On the other hand, these nanoparticles are not water-soluble so that cannot be directly used in many applications. Recently, transferring nanoparticles from an organic solution into an aqueous solution by ligand exchange is a common method. However, this process has the defect problem as mentioned earlier. Therefore, a good preparation of QD nanocrystals (NCs) must have the following key:

1. the direct synthesis of high-quality QDs in water solution without any harsh solvent exchange.
2. the development of methods for the assembly of individual nanodots into functional nano-architectures that are constructed from photo-stable nano-clusters.
3. the preparation of highly emissive gel or monoliths to meet specific color needs.

Recently, Prof. Kuan-Jiuh Lin and Dr. Fu from National Chung Hsing University found a less expensive, simpler and less toxic method to synthesize CdSe nanoparticles. They have developed a methodology for the directed self-assembly of anisotropic thiol-capped CdSe NCs from aqueous solutions into 3D solid-state architectures that reveal unique optical properties. Water-soluble CdSe NCs have been successfully synthesized via a green synthetic route using 3-mercaptoproionic acid (MPA) as the capping agent. Furthermore, the assembly of thiol-capped CdSe NCs from a solution into functional solid-state architectures was achieved using water-soluble PVA matrix as the stabilizer; this stabilizer can enhance the PL intensity and control the growth and morphology of the CdSe NCs during the photoactivation of CdSe QDs.

Same as the common CdSe nanoparticles, this sample has strong light stability, size-dependent emission peak, narrow bandwidth of emission peak, etc. Its various applications have been mentioned in the above section, in which light-emitting diodes and solar cells applications and it is necessary to fully understand the linear and nonlinear optical effect of material itself. We used the photoluminescence (PL) measurement system to measure the linear optical effect and the Z-scan system to measure its nonlinear optical effect.

Chapter2 Principles

2.1 Photoluminescence System

2.1.1 Photoluminescence System

Photoluminescence measurement is an indirect optical method to figure out the band structure and the carrier transportation behaviors in a material. The doping types, bandgap energy, composition of bulk material and the path of carrier transportation, lifetime of the nano-material can be identified in the photoluminescence spectrum. Therefore, the PL spectra of materials can be served to investigate the material quality and be a key technology of the development of nano-technology.^[29]

Luminescence is a phenomenon that physical system resulting electromagnetic radiation due to excessive radiation or intense heat. Typical light-emitting process for the light-emitting devices includes three steps: (1) Excitation, (2) Thermal equilibrium, (3) Recombination.

- (1) Excitation : When the light incident, if the photon energy of incident light is equal to or exceed the energy gap, it will stimulate the valence band electrons across the gap to the conduction band, and generate electron-hole pairs.
- (2) Thermal equilibrium : The electron in higher energy state of conduction band will come to the lowest energy state of conduction band by nonradiative relaxation.
- (3) Recombination : Finally, the electron in the conduction band will return to the

valence band by radiative relaxation and recombination with the hole.

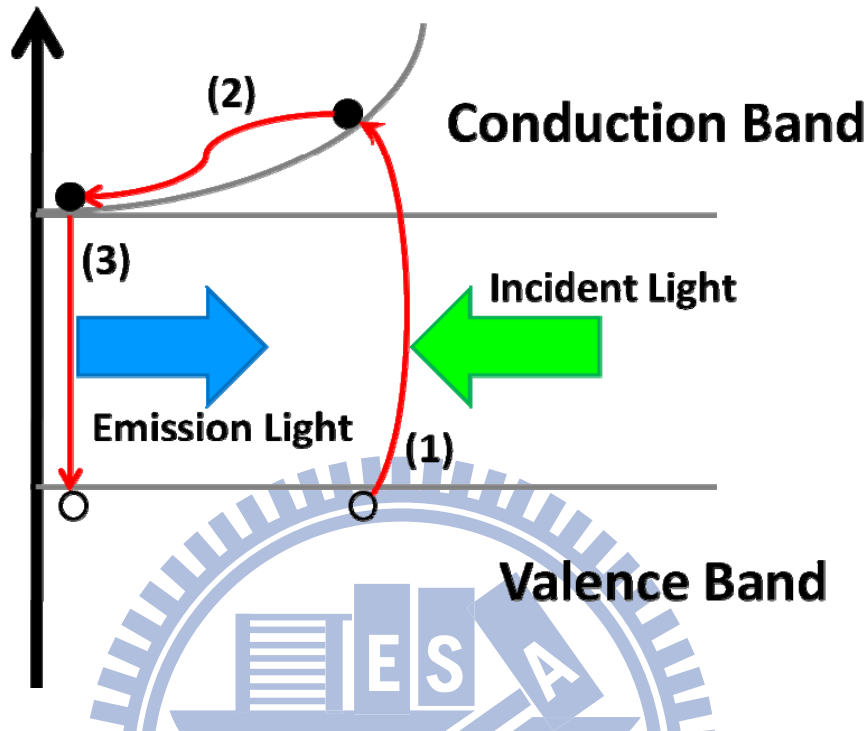


Fig. 2-1 (1) Excitation. (2) Thermal equilibrium. (3) Recombination.

In the bulk of a crystalline material, translational symmetry leads to the formation of electronic energy bands. Defects or impurities break the periodicity of the lattice and make a sub-band structure locally. The perturbation usually can be characterized by a discrete energy level that lies between the conduction and valence band. Depending on the defect or impurity, the state acts as a donor or acceptor of excess electrons in the crystal. Electrons or holes are attracted to the excess or deficiency of local charge due to the impurity nucleus or defect, and Coulomb binding occurs.^[30]

If the temperature is relatively low, carriers will be trapped at these states. When these carriers recombine radiatively, the energy of the emitted light can be analyzed to determine the energy of the defect or impurity level. (see Fig. 2-2)

The sub-levels, which lie near the conduction or valence band edge, are more likely to participate in radiative recombination.

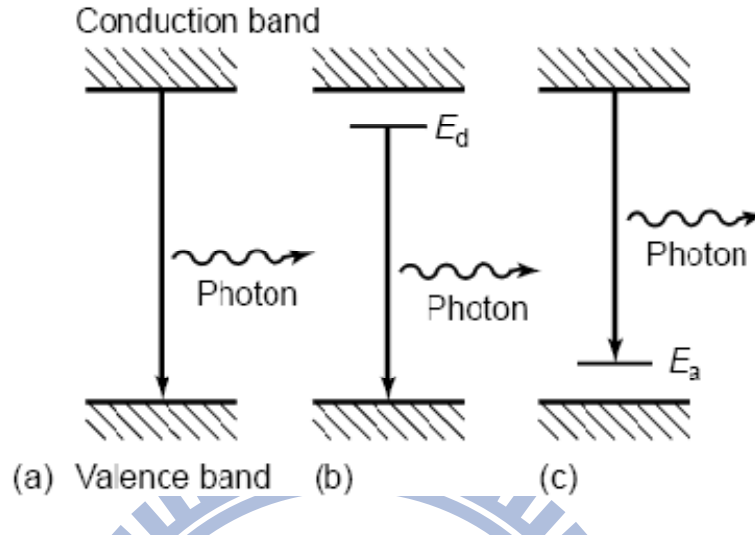


Fig. 2-2 Radiative recombination paths: (a) band-to-band; (b) donor to valence band; (c) conduction band to acceptor.^[30]

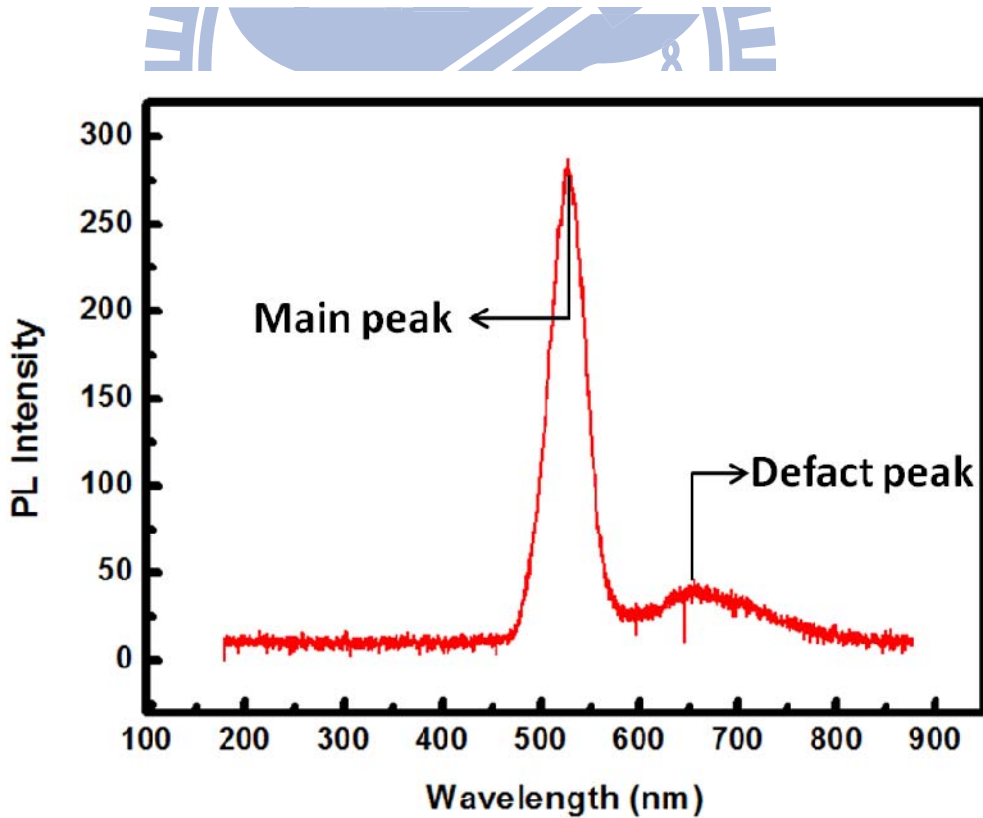


Fig. 2-3 A typical photoluminescence spectrum.

In a typical photoluminescence spectrum shown in Fig 2-3, there are two peaks, one for the main emission peak of the sample and the other one caused by the defect. Therefore, by analyzing the photoluminescence spectrum, the bandgap energy, impurity activation energy, and the contribution of defects can be identified. Furthermore, we can also get the information of the material structure, composition and quality which are difficult to get by general physical or electrical measurement method.

2.1.2 Time-resolved Photoluminescence System

The information of carrier dynamics, such as carrier recombination process and the fluorescence lifetime, can be obtained by measuring the time-resolved photoluminescence.^[29]

By using time-resolved photoluminescence system, we can also identify the different physical mechanism of fluorescence, especially for understanding the excitation and decay process of light-emitting material or component after the optical excitation. In addition, PL spectra from the different fluorescence decay process can be used to resolve the quantum structure of defects and quantum efficiency.

We used the ultrashort laser pulses to excite sample and the fluorescence photons were measured by the single-photon detector at a specific wavelength. After several counts in detector, the fluorescence photon probability distribution appears and this distribution curve corresponds to the excitation fluorescence intensity decay curve $I(t)$. (see Fig.2-4)

Due to the response time of the single-photon detectors, our temporal measurement accuracy is limited to be ~ 20 ps. Due to the high sensitivity of

single-photon detector, we could compare the efficiency and lifetime of different samples accurately. Since the intensity of pump pulses is very low, the nonlinear optical effect which often causes serious artifact in pump-probe measurement system, can be avoided for the time-resolved photoluminescence measurement system.

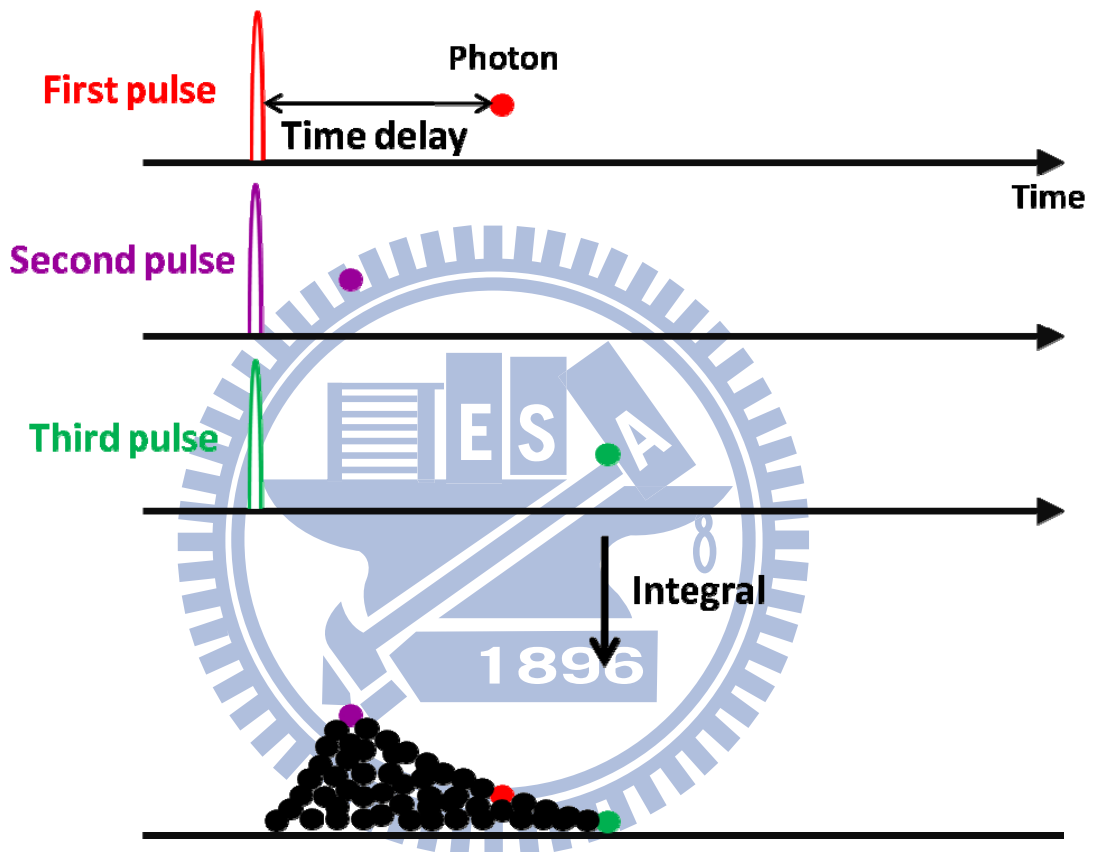


Fig. 2-4 The basic principle of time-resolved photoluminescence.

2.2 Z-scan System^[32,33,34]

2.2.1 Basic Principle of Z-scan

The nonlinear optical properties of semiconducting materials are being widely studied as potential components of various optical devices. There are many materials being observed large nonlinearities and used in demonstrating all-optical switching at incident photon energies nearly resonant with the energy gap of the material, such as InSb^[35], GaAs^[36], and HgCdTe^[37]. Large carrier nonlinearities are also observed in the transparency region where the carrier excitation mechanism is two-photon absorption.

Nonlinear interferometry, degenerate four-wave mixing, nearly degenerate three-wave mixing, ellipse rotation, and beam-distortion measurements are the typical techniques to measure nonlinear-optical properties of materials. But they need a complex experimental apparatus or precise beam scans followed by detailed wave-propagation analysis. Z-scan is a single-beam technique for measuring the sign and magnitude of nonlinearities that offers simplicity as well as high sensitivity. The demonstrated sensitivity to nonlinearly induced phase changes is better than $\lambda/100$.

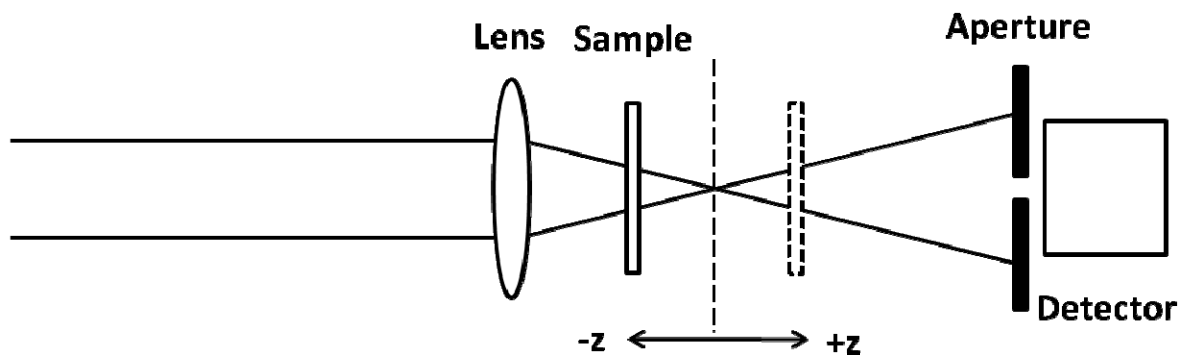


Fig. 2-5 Basic experimental setup of Z-scan.

The basic experimental setup of Z-scan is shown in Fig.2-5. Using a Gaussian laser beam in a tight focus-limiting geometry, the transmittance of a nonlinear medium through a finite aperture placed in the far field is measured as a function of the sample position (z) which is measured with respect to the focal plane. For this measurement, a thin material with a thickness much less than the beam depth of focus is placed normal to the incident beam on top of a translation stage and the changes in transmittance is measured as the sample is moved from $-Z$ to $+Z$ with a fine resolution.

Z-scan technique is to use single beam to measure the nonlinear refractive index and nonlinear absorption. When its intensity is strong enough, the incident beam through an optical medium induces a self-focusing or self-defocusing effects due to the optical Kerr effect. Under the intense photoexcitation, the dielectric constant ϵ changes with the electric field square imposed on the media. If we indicate it in term of the refractive index, the relation becomes

$$n = n_0 + \frac{n_2}{2} |E|^2 = n_0 + \gamma I \quad \text{Eq. 2-1}$$

where n_0 is linear refractive index,

E is Electric field strength,

I is power of laser beam with sample,

γ is nonlinear refractive index, and the nonlinear refractive index term is

$$n_2 = \frac{cn_0}{40\pi}$$

From Eq. 2-1, one can learn that if n_2 is positive, then the center of the sample has a higher refractive index and outer side has a smaller refractive index. Therefore, when the beam transmits through the sample, the sample behaves like a convex lens and then the beam will be focused. (see Fig. 2-6) On the other

hand, if n_2 is negative, the sample works as a concave lens, and the beam will be diverged. (see Fig. 2-7)

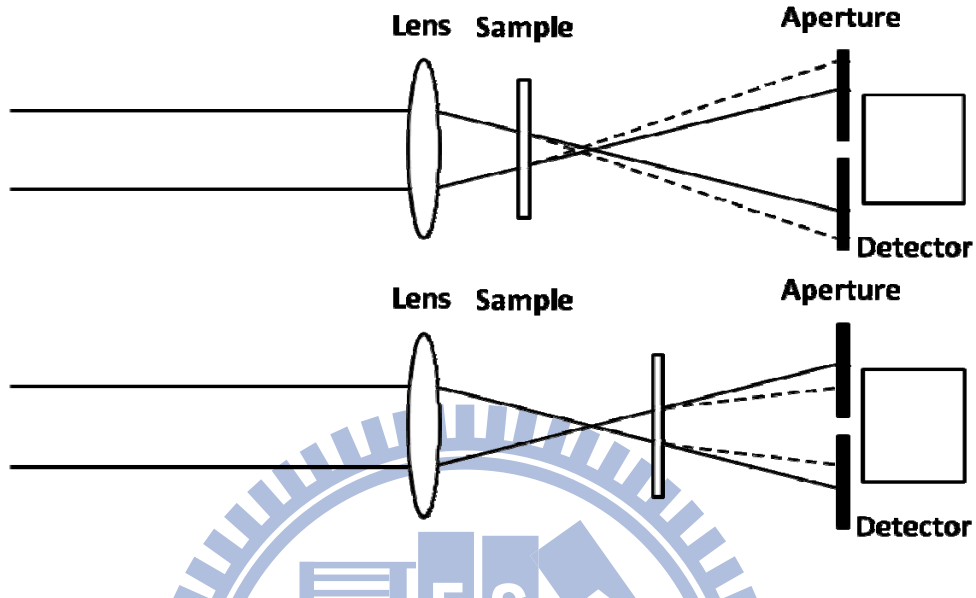


Fig. 2-6 If n_2 is positive, when we move the sample, will get different power of laser beam.

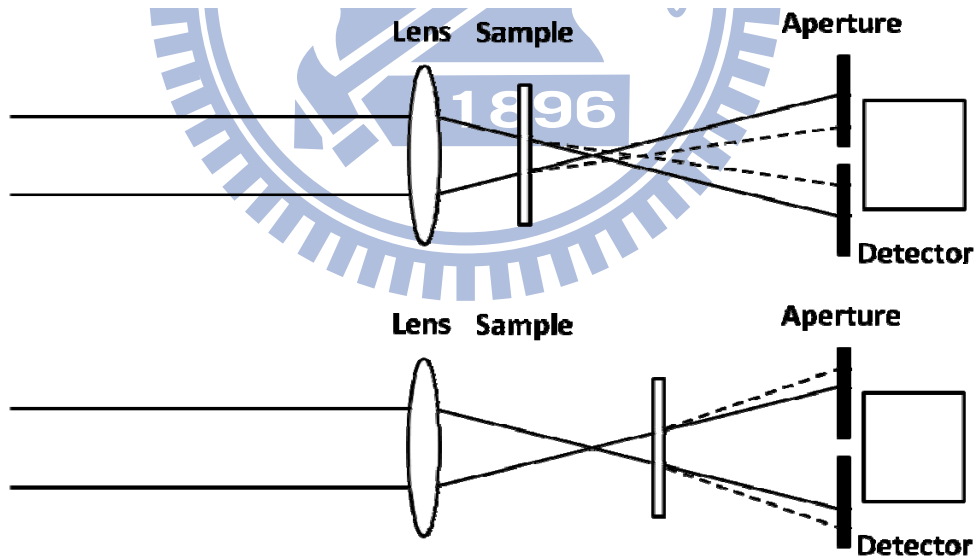


Fig. 2-7 If n_2 is negative, the laser beam diverges.

Therefore, when the laser beam hits the sample, and we move the sample from $+Z$ to $-Z$, then we will be able to get the data of transmittance change with the position Z , due to the self-focusing or self-defocusing effects.

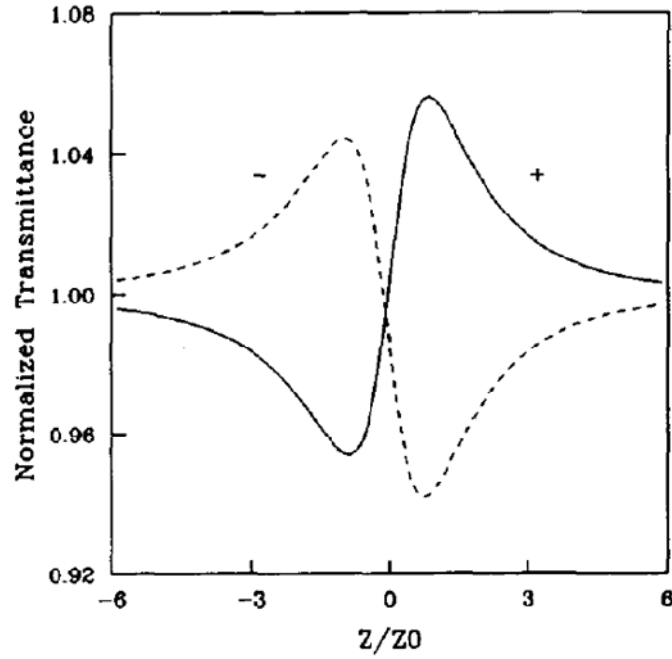


Fig. 2-8 The Z-scan data of transmittance change with Z/Z_0 .^[33]

The solid line in Fig. 2-8 is the case of the positive nonlinear refractive index (self-focusing material). At the $-Z$ position, self-focusing causes the focusing of the laser beam before the typical focusing position ($Z=0$), and then the light is more divergent than the original at the detector and the signal can be lower than that at $Z=0$. At $+Z$ position, the power of laser beam is stronger than the power at $Z=0$. Meanwhile, the dashed line represents the phenomena of the material with negative nonlinear refractive index (self-defocusing material). The result is exactly opposite to the self-focusing material.

Suppose the laser beam is a TEM_{00} Gaussian beam and the propagation direction is $+Z$, then the electric field can be expressed as follows

$$E(z, r, t) = E_0(t) \frac{w_0}{w(z)} \times \exp \left[-\frac{r^2}{w^2(z)} - \frac{ikr^2}{2R(z)} \right] e^{-i\phi(z,t)} \quad \text{Eq. 2-2}$$

where w_0 is the beam waist of TEM₀₀ Gaussian beam,

$w^2(z) = w_0^2 \left(1 + \frac{z^2}{z_0^2}\right)$ is the beam radius,

$R(z) = z \left(1 + \frac{z_0^2}{z^2}\right)$ is the radius of curvature of the wavefront at z ,

$z_0 = \frac{k w_0^2}{2}$ is the diffraction length(Rayleigh length) of the beam,

$k = \frac{2\pi}{\lambda}$ is the wave vector,

λ is the laser wavelength, and

$E_0(t)$ denotes the radiation electric field at the focus and contains the temporal envelope of the laser pulse. Here,

$e^{-i\phi(z,t)}$ term contains all the radially uniform phase variations.

If the thickness of the sample is thin enough ($L \ll Z_0$), then the changes in the beam diameter within the sample due to either diffraction or nonlinear refraction can be neglected. Such an assumption simplifies the problem considerably, and the amplitude \sqrt{I} and phase ϕ of the electric field as a function of z' are now governed a pair of simple equations:

$$\frac{d\Delta\phi}{dz'} = \Delta n(I)k \quad \text{Eq. 2-3}$$

$$\frac{dI}{dz'} = -\alpha(I)I \quad \text{Eq. 2-4}$$

here z' is the propagation depth in the sample.(not be confused with the sample position z) and

$\alpha(I)$ includes linear and nonlinear absorption terms.

Typically, when the nonlinear absorption is small enough, nonlinear terms can be ignored. Eq. 2-3 and Eq. 2-4 are solved to give the phase shift $\Delta\phi$ at the

exit surface of the sample which simply follows the radial variation of the incident irradiance at a given position of the sample z .

$$\Delta\phi(z, r, t) = \Delta\phi_0(z, t) \times \exp\left(-\frac{2r^2}{w^2(z)}\right) \quad \text{Eq. 2-5}$$

with

$$\Delta\phi_0(z, t) = \frac{\Delta\phi_0(t)}{1 + z^2/z_0^2} \quad \text{Eq. 2-6}$$

$$\Delta\phi_0(t) = k\Delta n_0(t) \times L_{\text{eff}} \quad \text{is the on-axis phase shift at the focus.} \quad \text{Eq. 2-7}$$

$$L_{\text{eff}} = \frac{1 - e^{-\alpha L}}{\alpha} \quad \text{and}$$

L is the sample length.

α is the linear absorption coefficient and

$$\Delta n_0 = \gamma I_0(t) \quad \text{with } I_0(t) \text{ being the on-axis irradiance at focus (i.e., } z = 0\text{).}$$

So, the complex electric field exiting the sample E_e now contains the nonlinear phase distortion.

$$E_e(z, r, t) = E(z, r, t) \times e^{-\alpha L/2} \times e^{i\Delta\phi(z, r, t)} \quad \text{Eq. 2-8}$$

We can decompose the complex electric field at the exit plane of the sample into a summation of Gaussian beams through a Taylor series expansion of the nonlinear phase term $e^{i\Delta\phi(z, r, t)}$ in Eq. 2-8.

$$e^{i\Delta\phi(z, r, t)} = \sum_{m=0}^{\infty} \frac{[i\Delta\phi_0(z, t)]^m}{m!} \times e^{-2mr^2/w^2(z)} \quad \text{Eq. 2-9}$$

Now, we can derive the resultant electric field E_a pattern at the aperture as

$$E_a(r, t) = E(z, r = 0, t) \times e^{-\alpha L/2} \times \sum_{m=0}^{\infty} \frac{[i\Delta\phi_0(z, t)]^m}{m!} \times \frac{w_{m_0}}{w_m} \times \exp\left(-\frac{r^2}{w_m^2} - \frac{ikr^2}{2R_m} + i\theta_m\right) \quad \text{Eq. 2-10}$$

here d is defined as the propagation distance in free space from the sample to the aperture plane. Assume $g = 1 + d/R(z)$, then

$$w_{m_0}^2 = \frac{w^2(z)}{2m+1}$$

$$d_m = \frac{k w_{m_0}^2}{2}$$

$$w_m^2 = w_{m_0}^2 \left[g^2 + \frac{d^2}{d_m^2} \right]$$

$$R_m = d \left[1 - \frac{g}{g^2 + d^2/d_m^2} \right]^{-1}$$

$$\theta_m = \tan^{-1} \left[\frac{d/d_m}{g} \right]$$

In Z-scan mathematical calculations, this method is quite useful, because in Eq. 2-10, we only need a sum of several term to get the electric field E_a . And this method is also easily extended to higher order nonlinearities.

Then the transmitted power through the aperture can be got by integrating $E_a(r, t)$ with the aperture radius r_a ,

$$P_T = c\varepsilon_0 n_0 \pi \int_0^{r_a} |E_a|^2 r dr \quad \text{Eq. 2-11}$$

n_0 is linear refractive index and ε_0 is the permittivity of vacuum.

Including the pulse temporal variation, the normalized Z-scan transmittance $T(z)$ can be calculated as

$$T(z) = \frac{\int_{-\infty}^{\infty} P_T dt}{S \int_{-\infty}^{\infty} P_i(t) dt} \quad \text{Eq. 2-12}$$

$P_i(t) = \frac{\pi w_0^2 I_0(t)}{2}$ is the instantaneous input power (within the sample).

$S = 1 - \exp\left(\frac{-2r_a^2}{w_a^2}\right)$ is the aperture linear transmittance.

w_a denoting the beam radius at the aperture in the linear regime.

Next, we define an parameter $\Delta T_{p-v} = T_p - T_v$ as the difference between the normalized peak and valley transmittance.(see Fig. 2-8) According to the Sheik-Bahae's paper ,

$$\Delta T_{p-v} \cong 0.406(1-s)^{0.25} |\Delta\phi_0| \text{ for } |\Delta\phi_0| < \pi. \quad \text{Eq. 2-13}$$

Then we can get Δn and n_2 from Eq. 2-13 & Eq. 2-7.

2.2.2 Effects of Nonlinear Absorption

In a large refractive nonlinearities material, commonly we can find single or two-photon absorption. The nonlinear absorption in such materials arising from either direct multiphoton absorption, saturation of the single photon absorption, or dynamic free-carrier absorption have strong effects on the measurements of nonlinear refraction using the Z-scan technique. With $S=1$, the nonlinear refraction is insensitive to Z-scan, so the coefficients of nonlinear absorption can be easily calculated from such transmittance curves.

The third-order nonlinear susceptibility is now considered to be a complex quantity

$$\chi^{(3)} = \chi_R^{(3)} + i\chi_I^{(3)} \quad \text{Eq. 2-14}$$

$\chi_I^{(3)} = \frac{n_0^2 \epsilon_0 c^2}{\omega} \beta$ the imaginary part is related to the 2PA coefficient β .

$\chi_R^{(3)} = 2n_0^2 \epsilon_0 c \gamma$ the real part is related to γ .

In Eq. 2-3,2-4 & Eq. 2-5, we ignore the nonlinear absorption, because it is small enough. Now we begin to consider it.

$$\alpha(I) = \alpha + \beta I \quad \text{Eq. 2-15}$$

After a similar calculation, we can get the transmitted power through the aperture

$$P(z, t) = P_i(t) \times e^{-\alpha L} \times \frac{\ln[1 + q_0(z, t)]}{q_0(z, t)} \quad \text{Eq. 2-16}$$

$$q_0(z, t) = \beta I_0(t) L_{\text{eff}} / (1 + z^2/z_0^2)$$

$P_i(t)$ was defined in Eq. 2-12.

For a temporally Gaussian pulse, Eq. 2-16 can be time integrated to give the normalized energy transmittance

$$T(z, S = 1) = \frac{1}{\sqrt{\pi} q_0(z, 0)} \quad \text{Eq. 2-17}$$

For $|q_0| < 1$, this transmittance can be expressed in terms of the peak irradiance in a summation form more suitable for numerical evaluation

$$T(z, S = 1) = \sum_{m=0}^{\infty} \frac{[-q_0]^m}{(m+1)^{3/2}} \quad \text{Eq. 2-18}$$

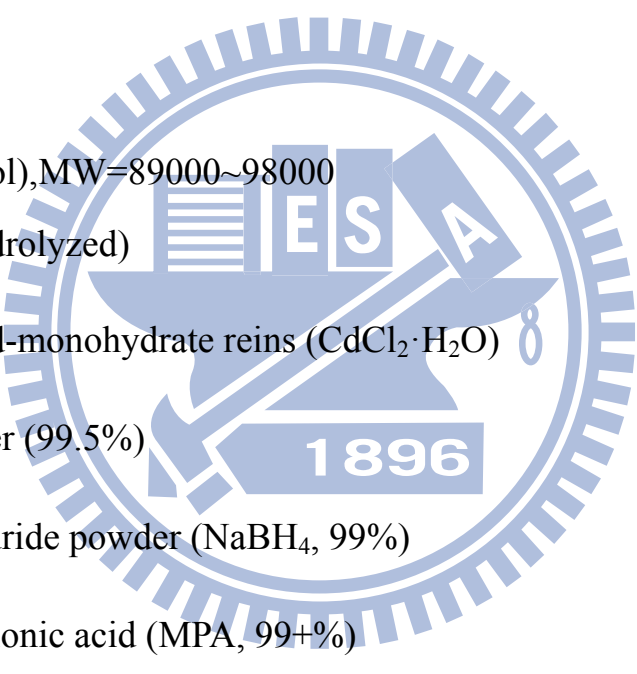
Therefore, by Eq. 2-18, when we get the open aperture (s=1) Z-scan data, we can get the two photon absorption coefficient β from Eq. 2-18 with the open aperture (S=1) Z-scan data.

Chapter3 Sample Preparation

All CdSe samples were prepared by Dr. Fu in Prof. Kuan-Jiuh Lin' lab in National Chung Hsing University. The sample preparation processes in this Chapter are from Dr. Fu's recent publication.^[38,39]

3.1 Preparation of the CdSe Nanoparticle

3.1.1 Materials :



poly(viny alcohol),MW=89000~98000 (PVA, 99 % hydrolyzed)	Aldrich
Cadmiumchlorid-monohydrate reins ($\text{CdCl}_2 \cdot \text{H}_2\text{O}$)	Aldrich
Selenium powder (99.5%)	Aldrich
Sodium borohydride powder (NaBH_4 , 99%)	Acros
3-mercaptopropionic acid (MPA, 99+%)	Aldrich
Coumarin-1 (99%)	Acros
Tris(hydroxymethyl)aminomethane (TRIS)	AMRESCO [®]
1,2-ethylene diphosphonic acid(EDPA)	Alfa Aesar

3.1.2 Procedure

1. Se precursor : Preparation of sodium hydrogen selenide.

Added 13.2 mg (0.2 mmol) of sodium borohydride (NaBH_4) and 10.4 mg (0.13 mmol) of selenium powder were to a 10-mL of two-necked flask. And then, cooled with ice bath; air in the system was then pumped-out and replaced with nitrogen gas.

Next, 1 mL of ultrapure water was added through a syringe. After 3 hours at 4 °C, the black selenium powder disappeared, and a clear NaHSe solution was obtained. The typical concentration of NaHSe was 0.1 mM.

2. Cd precursor :

A mixture of $\text{CdCl}_2 \cdot \text{H}_2\text{O}$ (46.5 mg, 0.2 mmol), MPA (17 μl , 0.2 mmol), and EDPA (4.75 mg, 0.025 mmol) was dissolved in 20 mL of N_2 -saturated ultrapure water. The solution was adjusted to pH 12 with 1M NaOH, and then was de-aerated with N_2 for 30 min.

3. Synthesis of CdSe nanoparticles :

CdSe nanoparticles were prepared by refluxing $\text{CdCl}_2 \cdot \text{H}_2\text{O}$ and NaHSe precursor in the presence of a mixed ligand system (MPA and EDPA). The molar ratio of Cd:MPA:EDPA:NaHSe was fixed at 8:8:1:1. An oxygen-free NaHSe solution (0.25 mL, 0.13 mM) prepared by step 1 was quickly injected into the mixture prepared by step 2 accompanied by vigorous stirring. And then, refluxed the mixture at 90 °C for 240 min.

4. Purification :

The as-synthesized CdSe nanoparticles were isolated by adding an ethanol/acetone (2:1 v/v) co-solvent. After CdSe nanoparticles precipitating,

centrifuged the solution at 4000 r/min for 10 min. Then repeated the above steps three times, the last time replaced by acetone to facilitate drying. Finally, added the purified CdSe nanoparticles into 0.25 M pH = 8.8 Tris-HCl buffer.

5. Formation of CdSe@PVA gels.

For gelation, a mixture of CdSe in 0.25 M of TRIS-HCl buffer (0.2 mL) and 0.6 mL of 5% (w/v) PVA in H₂O was stirred at room temperature under ambient fluorescent lighting for 43 h.

6. Preparation of CdSE@PVA.

- (1) CdSe 1.0 ml + PVA 3 ml, stirred for 1 hr
- (2) in over vacuum at 60 oC for 4 hrs.
- (3) Then wait for 1 day
- (4) Hydrothermal at 60 oC for 6 hrs, wait 2 days in air.
- (5) Then immersed in water for 52 hrs
- (6) in over vacuum at 60 oC for 4 hrs.
- (7) The final production

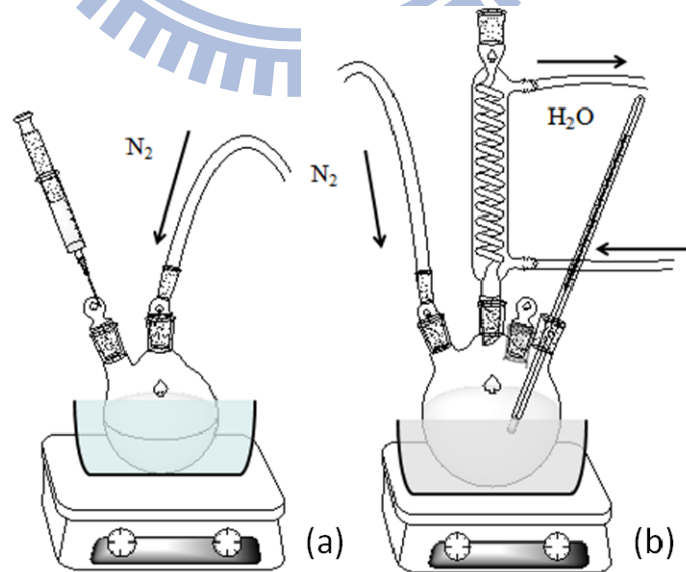


Fig. 3-1 (a) Se precursor (b) Se precursor.

3.2 List of Samples

Sample	Type	CdSe	PVA	Buffer
A	CdSe with buffer			tris-HCl
B	CdSe with buffer			PBS
C	Pure CdSe			
D	Pure CdSe			
E	CdSe@PVA gel	1 ml	0.5 ml	tris-HCl
F	CdSe@PVA gel	1 ml	3 ml	tris-HCl
G	CdSe@PVA gel	0.2 ml	2 ml	tris-HCl
H	CdSe@PVA gel	0.2 ml	6 ml	tris-HCl
I	CdSe@PVA gel	1 ml	3 ml	PBS
J	CdSe@PVA film	1 ml	3 ml	

Chapter4 Experiment & Result

4.1 Photoluminescence and Time-resolved Photoluminescence System

4.1.1 Experiment Setup

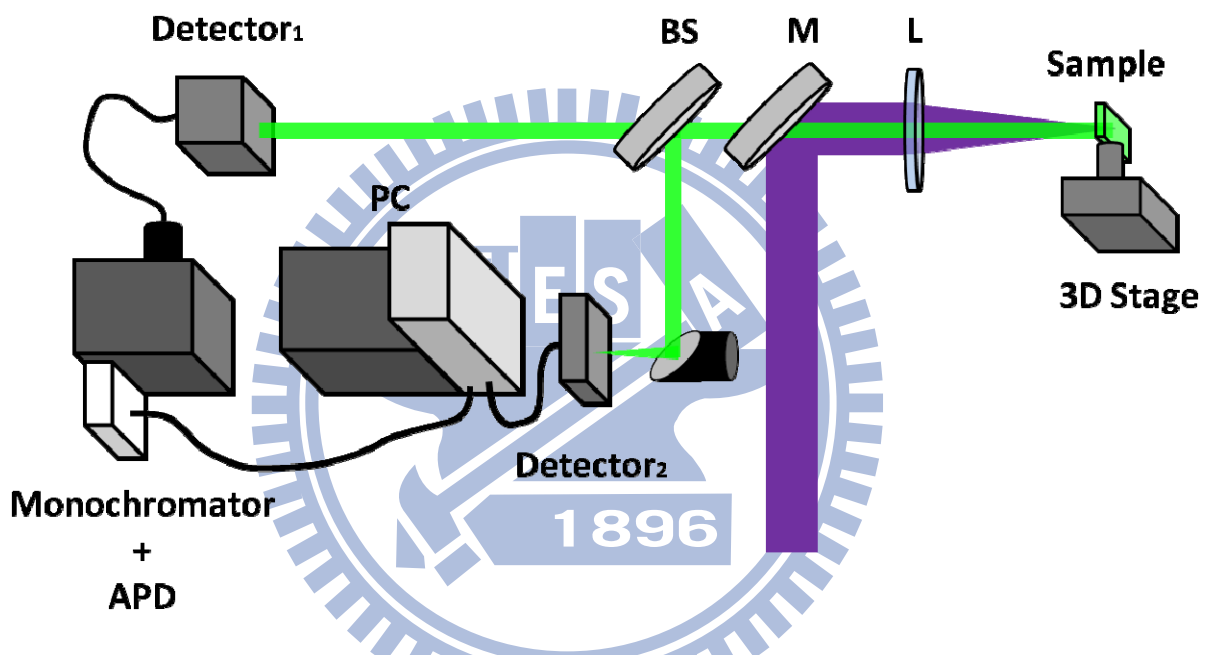


Fig. 4-1 Photoluminescence and time-resolved photoluminescence system setup.

1. Excitation Laser : Ti:Sapphire Laser from Coherent (Chameleon), center wavelength: 700~890nm, max power: 2 W pulse width: 120fs, repetition rate: 82MHz. For above bandgap energy excitation, 350~445 nm laser pulses were obtained by using the second harmonic generation technique.
2. M : dichroic mirror.
3. L : focusing lens.

4. BS : beam-splitter.
5. Detector₁ : USB2000 Miniature Fiber Optic Spectrometer. Use to measure the PL spectrum.
6. Detector₂ : measure the TR-PL data.
7. Monochromator : MS257 from Newport. It is a completely automated, efficient 1/4 m instrument, with enough versatility to satisfy most spectroscopy applications.
8. APD : single-photon detector from MPD

The setup of the photoluminescence and time-resolved photoluminescence system is shown in Fig. 4-1. A Ti:Sapphire laser or an amplified Ti:Sapphire laser is used to drive this system. The laser pulses with the center wavelength at 800 nm are frequency-doubled by using a nonlinear crystal BBO to photoexcite the samples above the bandgap energy. Emitted light from the sample is divided into two paths, one to photoluminescence system and the other one to time-resolved photoluminescence system. Time-resolved PL is measured by using single-photon counting method, while time-integrated PL is measured by a spectrometer with photodiode array.

4.1.2 Result

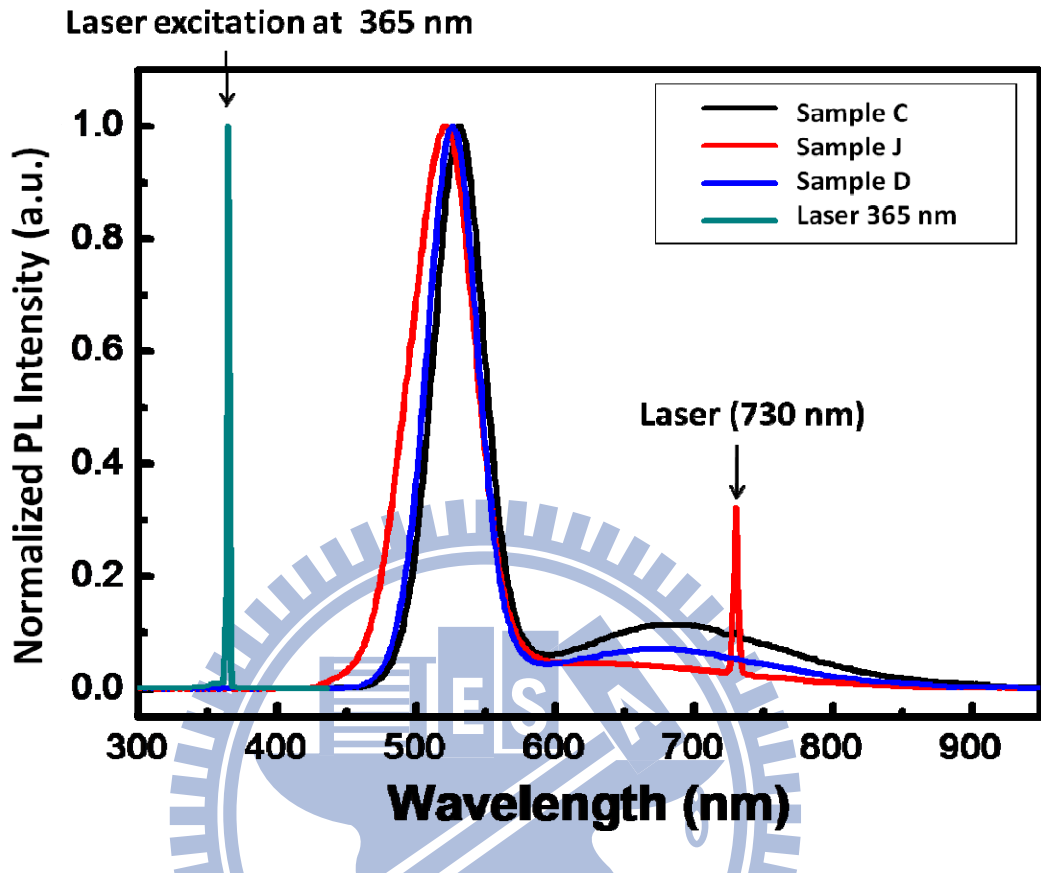


Fig. 4-2 Normalized PL intensity of sample C , D , J.

Fig. 4-2 shows the normalized PL intensity of three different samples. The sample C and D are pure CdSe nanoparticles with water, respectively and prepared with different reaction time in synthesis. The peak position of sample C locates at a longer wavelength that that of sample D. Since the reaction time of sample C is longer than that of sample D, the particle size of sample C is supposed to be larger than that of sample D and the shifted PL peak position of sample C and D may be due to the different particle sizes. Because of Size Quantization Effect, the peak position of sample D is red-shifted. Sample J has the same composition with sample C, but adding PVA and in the form of film so that there is no water in this PVA film. Besides the main peak, samples C and D

have another weak and broad peak at the longer wavelength sides. This broad peaks may be due to the defects existing on the surface of CdSe nanoparticles .^[40] Sample J does not have apparent defect-related PL peak.

Next, we expose the sample C and J to UV light source, and compare the PL spectrums at different excitation times.

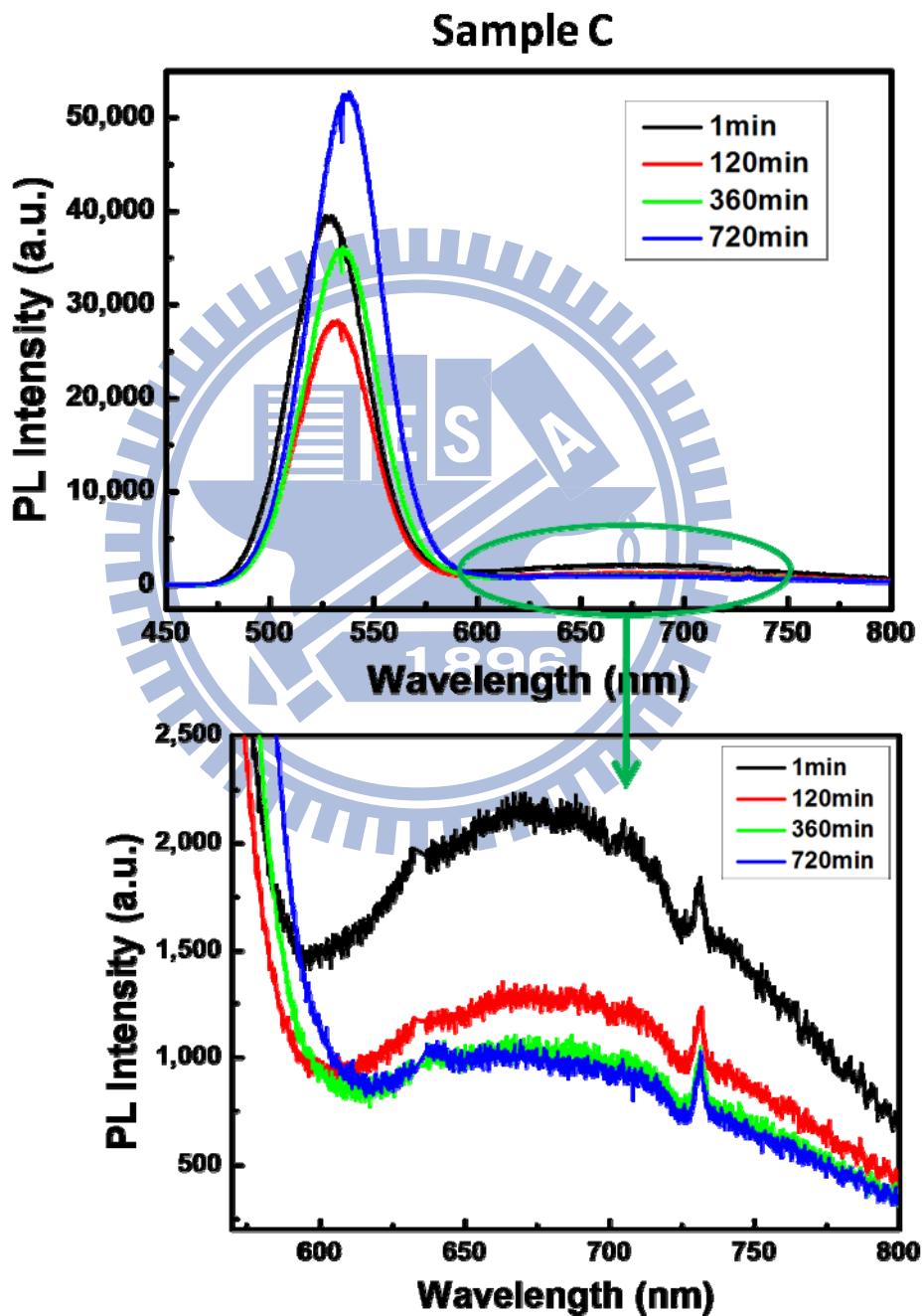


Fig. 4-3 PL spectrum of sample C with different excitation times.

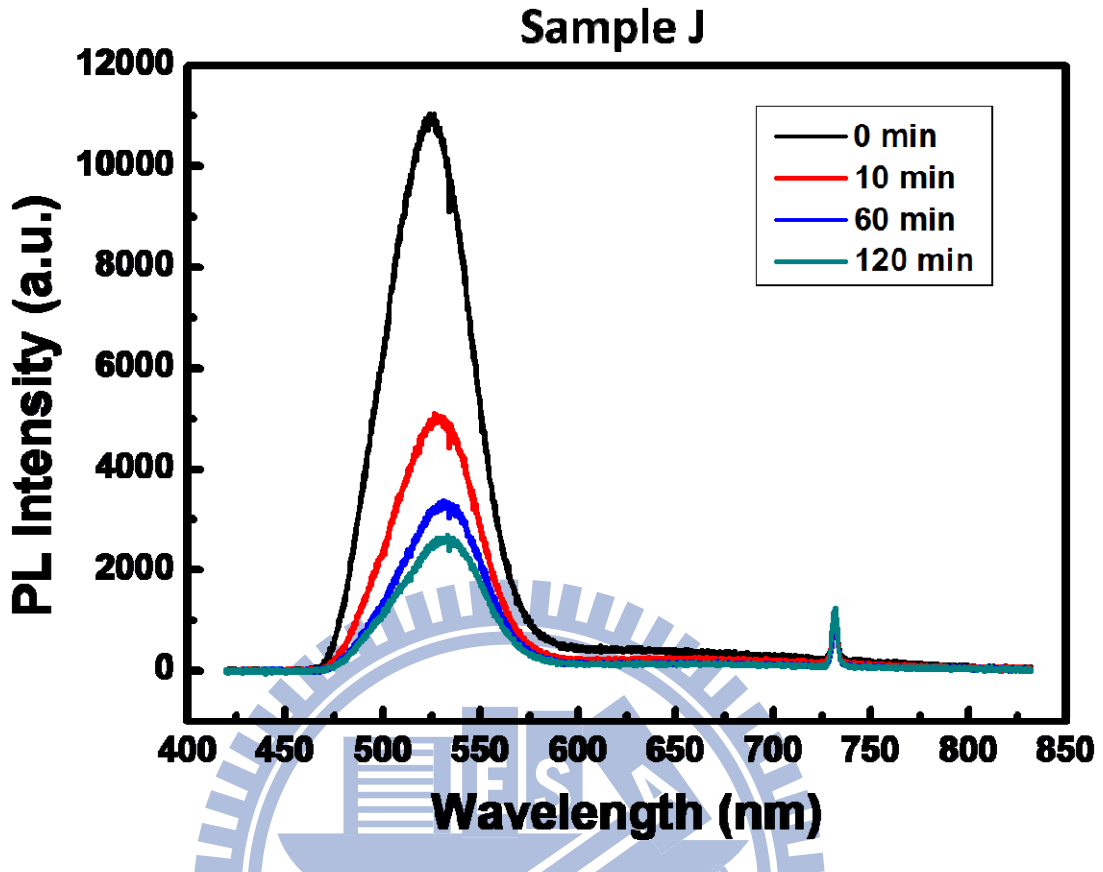


Fig. 4-4 PL spectrum of sample J with different excitation times.

In Fig. 4-3, we can find that the defect-related PL peak of sample C becomes smaller with the increase excitation time, while the main PL peak intensity first decreases and then increases as the exposure time increases. For sample J, however, the main peak intensity continuously decreases with the increase of exposure time and there was no significant defect-related peak. We refer this phenomena to “**Photoactivation theory**”^[40,41].

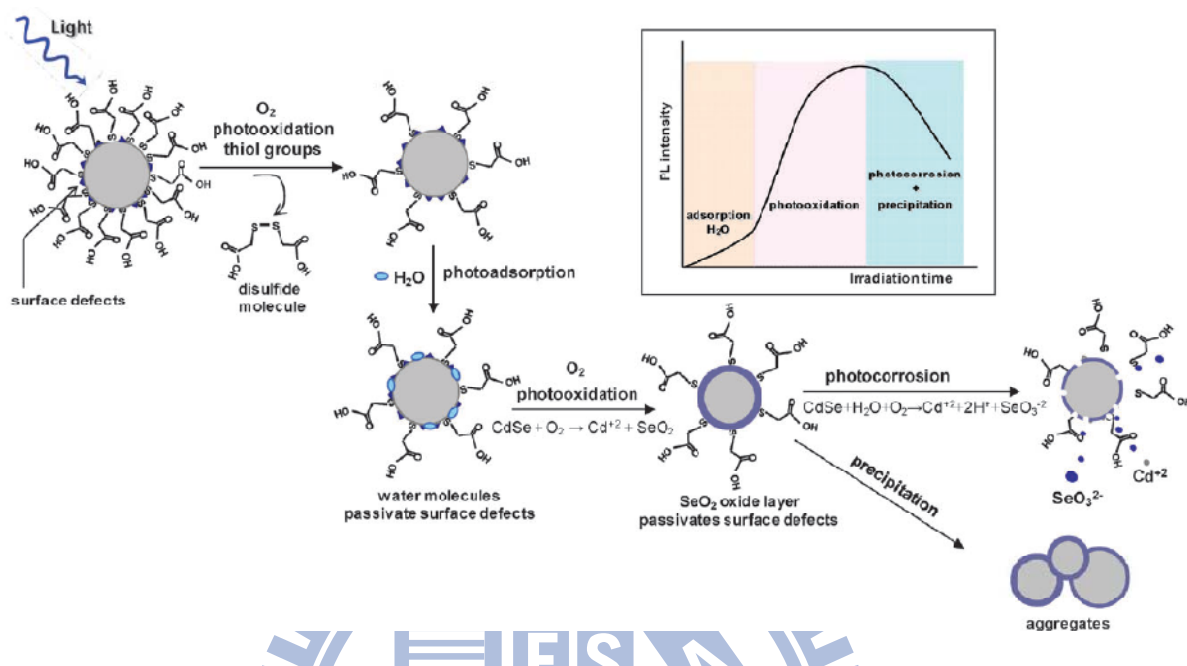
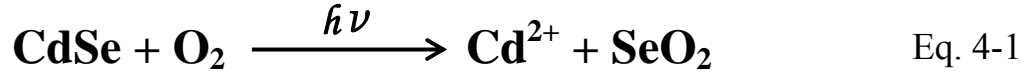


Fig. 4-5 Schematic picture of the mechanism of the photoactivation reaction occurring on water-soluble CdSe nanoparticles and changes on PL intensity observed during this pathway.

The Photoactivation of water-soluble nanoparticles can be broadly divided into three steps.

1. By photo-oxidation, the surface thiol groups produce disulfide molecules, which are water-soluble and readily removed from the nanoparticles surface and dissolved into the aqueous solution. And then nanoparticles will stick together to form aggregates of nanoparticles. In this process, H_2O or surfactant molecules have probability to be absorbed to the nanoparticles surface and passivate surface defects. As a result, PL intensity gradually increases.

2. Photo-oxidation of the nanoparticles surface to form a SeO_2 layer as a result of the transfer of absorbed energy to the surface of nanoparticles and following oxidation of surface Se.



This oxide layer passivates the surface defects and leads to a large increase in photoluminescence.

3. When the excitation times become very long, oxidative dissolution of the nanoparticles occurs and SeO_3^{2-} and Cd^{2+} ion are desorbed from the QD surface.



The SeO_2 layer gradually disintegrates, and exposes to new surface defects. As the nanoparticle surface is destroyed gradually, the PL intensity also decrease gradually.

While the similar process is observed for sample C in Fig. 4-2, in the case of sample J, the photoactivation process was not obviously observed in sample J in the form of film without water molecules.

Next, in order to understand the relation between photoactivation and CdSe/PVA ratio, we compare the PL spectrums of four samples with different CdSe/PVA ratios.

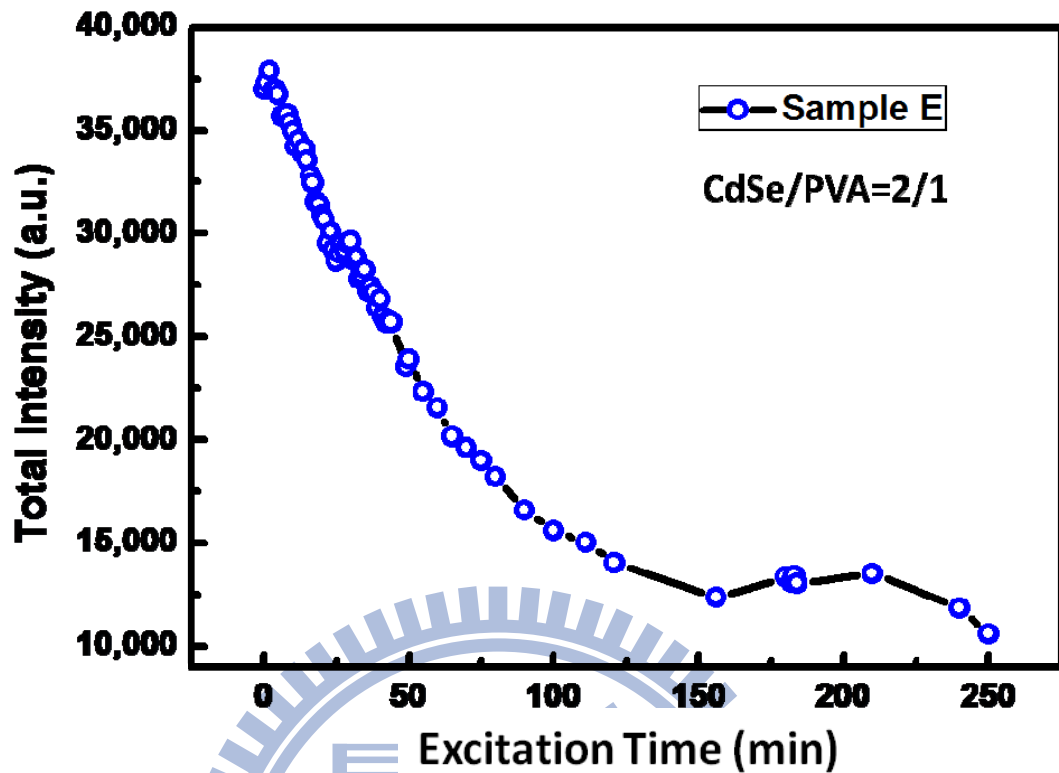


Fig. 4-6 Total PL intensity change with excitation time of sample E.

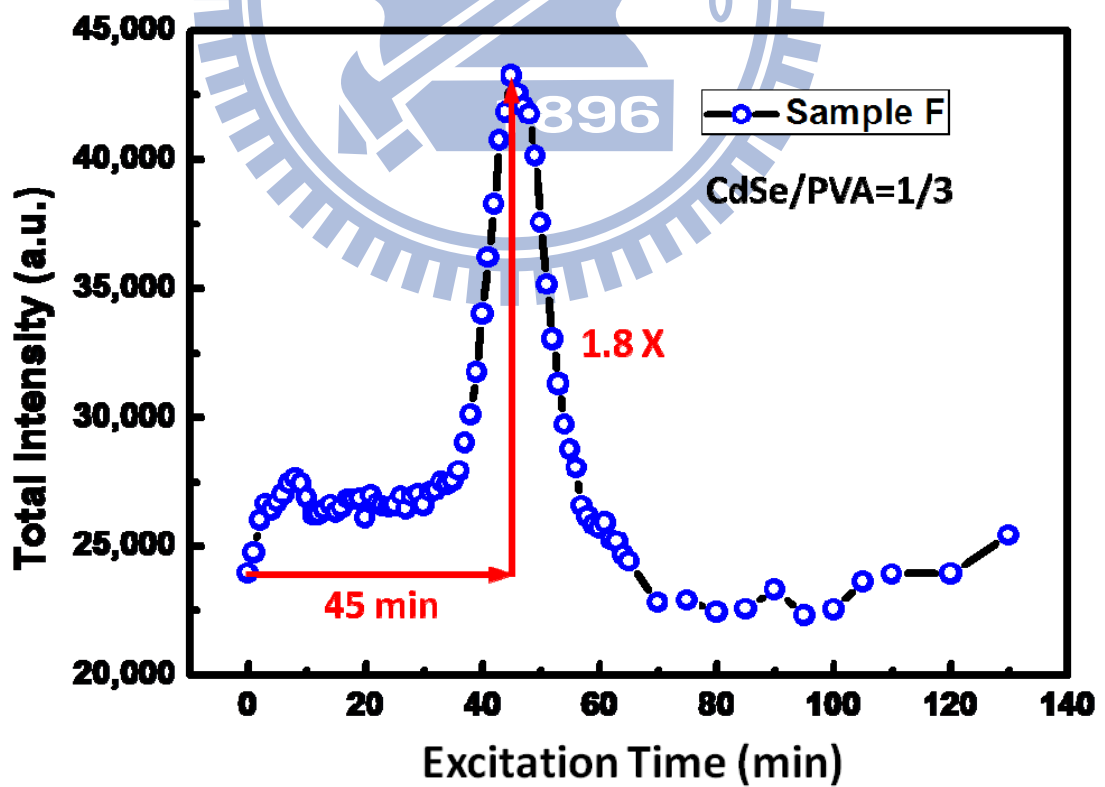


Fig. 4-7 Total PL intensity change with excitation time of sample F.

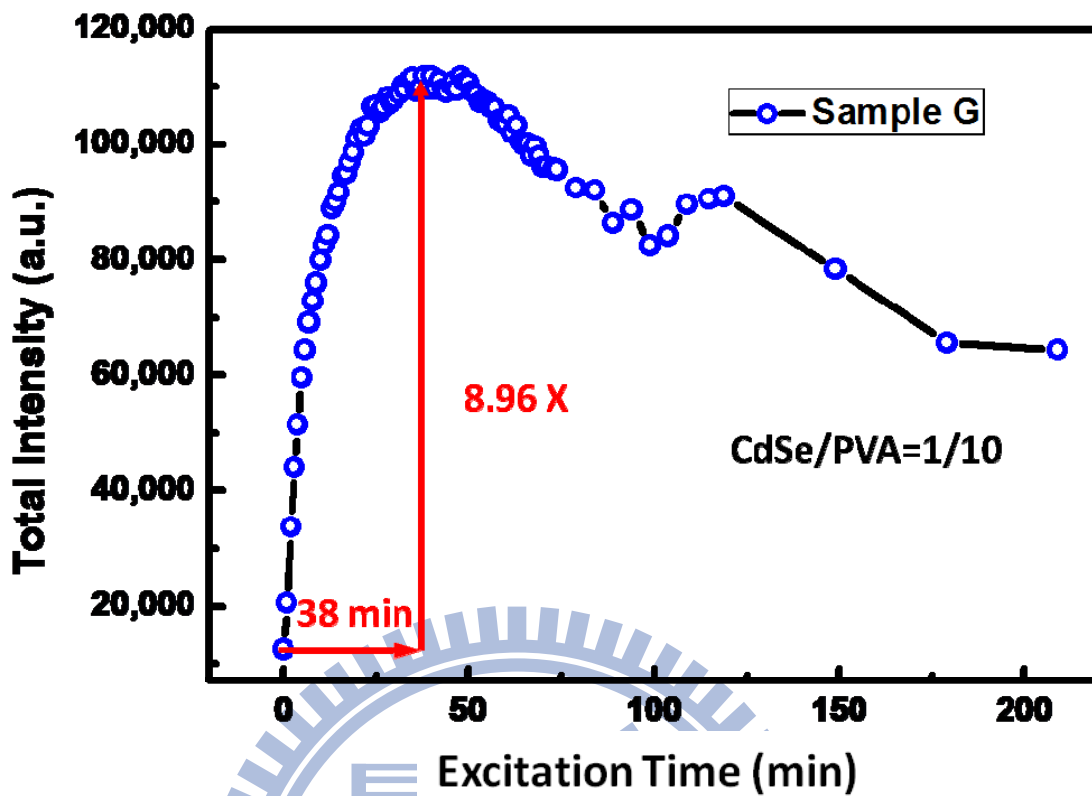


Fig. 4-8 Total PL intensity change with excitation time of sample G.

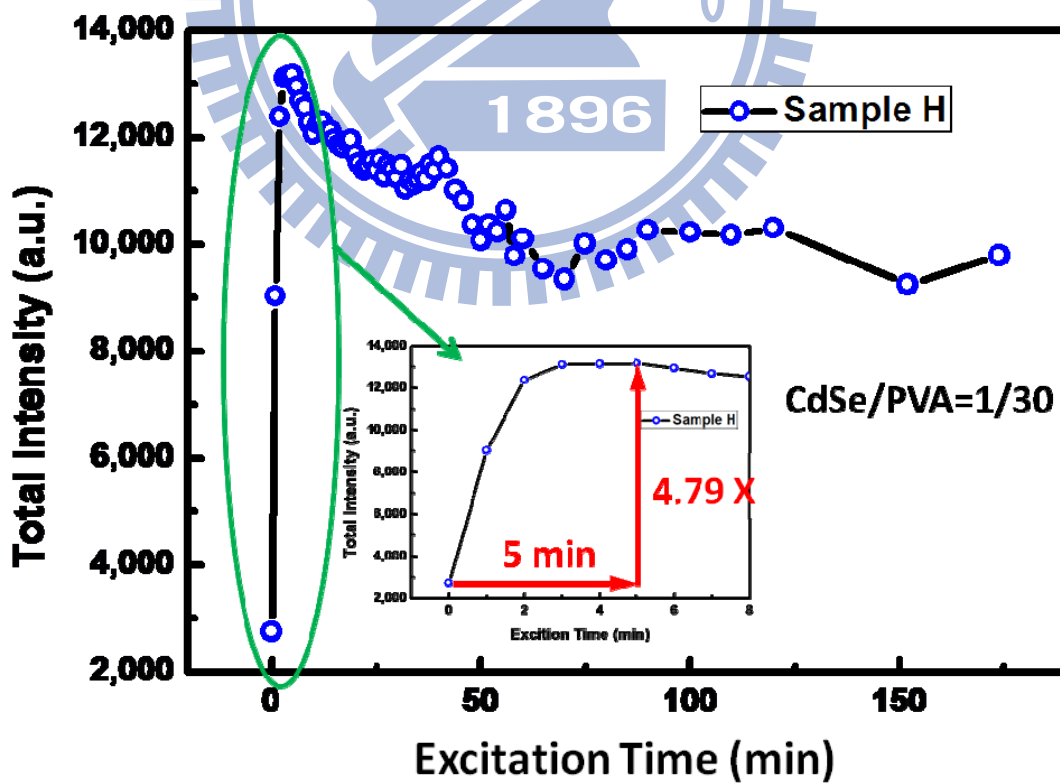


Fig. 4-9 Total PL intensity change with excitation time of sample H.

Fig. 4-6~4-9 show the total PL intensity versus excitation time of samples E, F, G, and H. The samples E, F, G, and H have different CdSe/PVA ratio, 2/1, 1/3, 1/10, 1/30, respectively. The PL intensities of samples F, G, and H increase by photoactivation, while that of sample E monotonically decreases as the excitation time increases. The enhancement of PL intensity in sample F, G, and H are $\times 1.8$, $\times 8.96$, $\times 4.79$ after light exposure of 45 min, 38 min, 5 min, respectively and the highest enhancement was observed for sample G (CdSe: PVA = 1:10). (see in Fig. 4-7)

Meanwhile, the high CdSe ratio (sample E, and F) will lead to the quenching effect and reduce the PL intensity. In the case of low concentration of CdSe, although the quenching effect is not obvious, the particles are too far away from each other so that the enhancement is still difficult.^[42] Our results show that the sample G has the best ratio of CdSe/PVA to balance these problems and enhance the PL intensity. For sample G, the concentration of PVA is large enough and after photoactivation PVA can protect CdSe nanoparticles effectively and prevent disintegration of SeO₂ layer. Therefore, the oxidative dissolution is less obvious and the PL intensity decays slowly. So, we propose a modified process for our case (see Fig. 4-10).

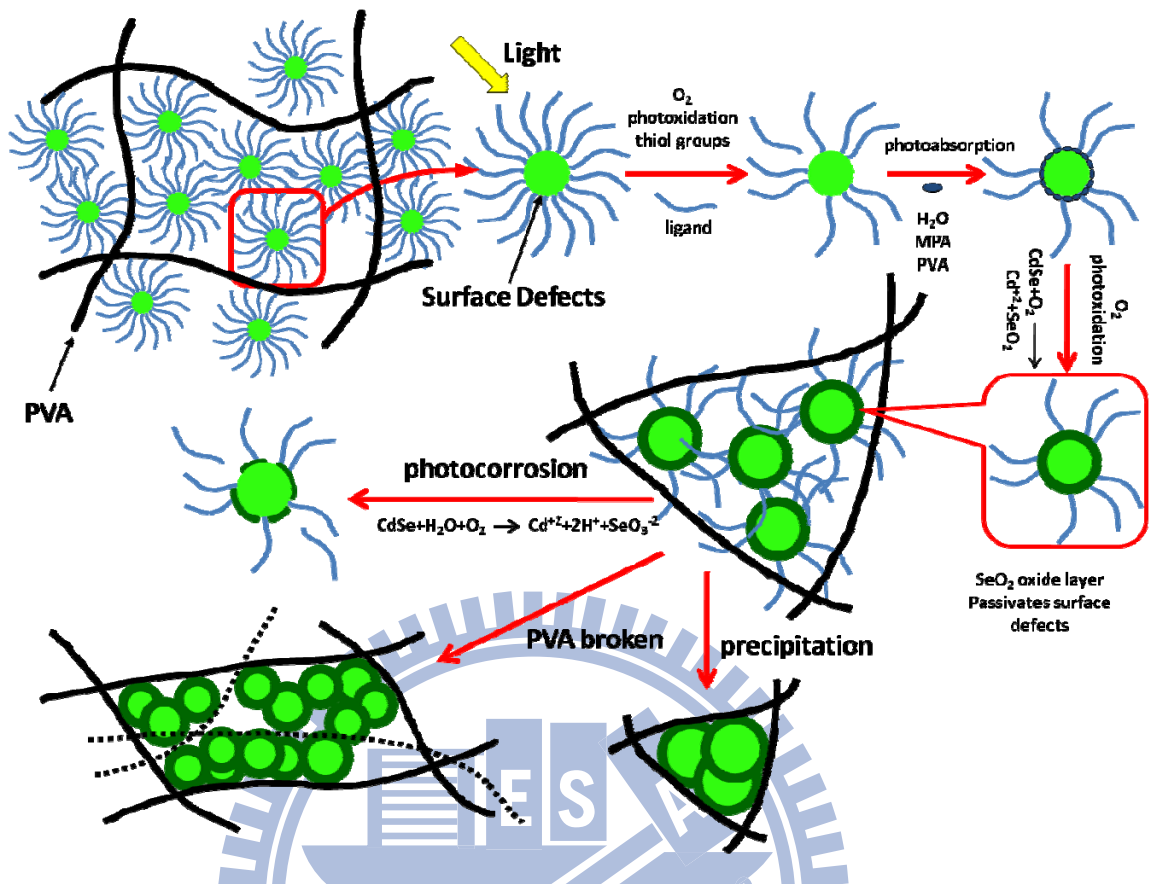
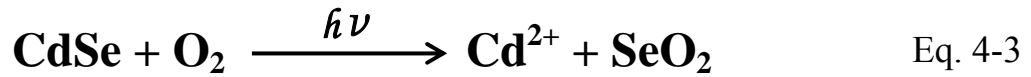


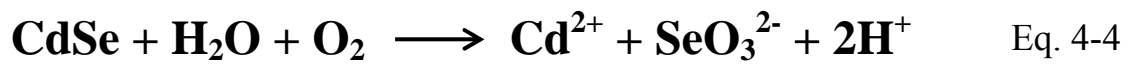
Fig. 4-10 Modified photoactivation reaction.

1. The CdSe nanoparticles are capped by PVA. By photo-oxidation, the surface thiol groups produce disulfide molecules, which are water-soluble and readily removed from the nanoparticles surface and dissolved into the aqueous solution. And then nanoparticles will stick together to form aggregates of nanoparticles. In this process, H₂O, PVA or surfactant molecules have probability to be absorbed to the nanoparticles surface and passivate surface defects. As a result, PL intensity gradually increases.
2. Photo-oxidation of the nanoparticles surface to form an SeO₂ layer as a result of the transfer of absorbed energy to the surface of nanoparticles and following oxidation of surface Se.



This oxide layer passivates the surface defects and leads to a large increase in photoluminescence.

3. When the excitation times become very long, oxidative dissolution of the nanoparticles occurs and SeO_3^{2-} and Cd^{2+} ion are desorbed from the QD surface.



The SeO_2 layer gradually disintegrate, and exposes to new surface defects. As the nanoparticles surface is destroyed gradually, the PL intensity also decrease gradually.

4. If we expose the CdSe nanoparticles to UV light source in a very long time. The “wall” form of PVA between CdSe nanoparticles will be broken by the laser pulses. And then nanoparticles will stick together to form aggregates of nanoparticles.

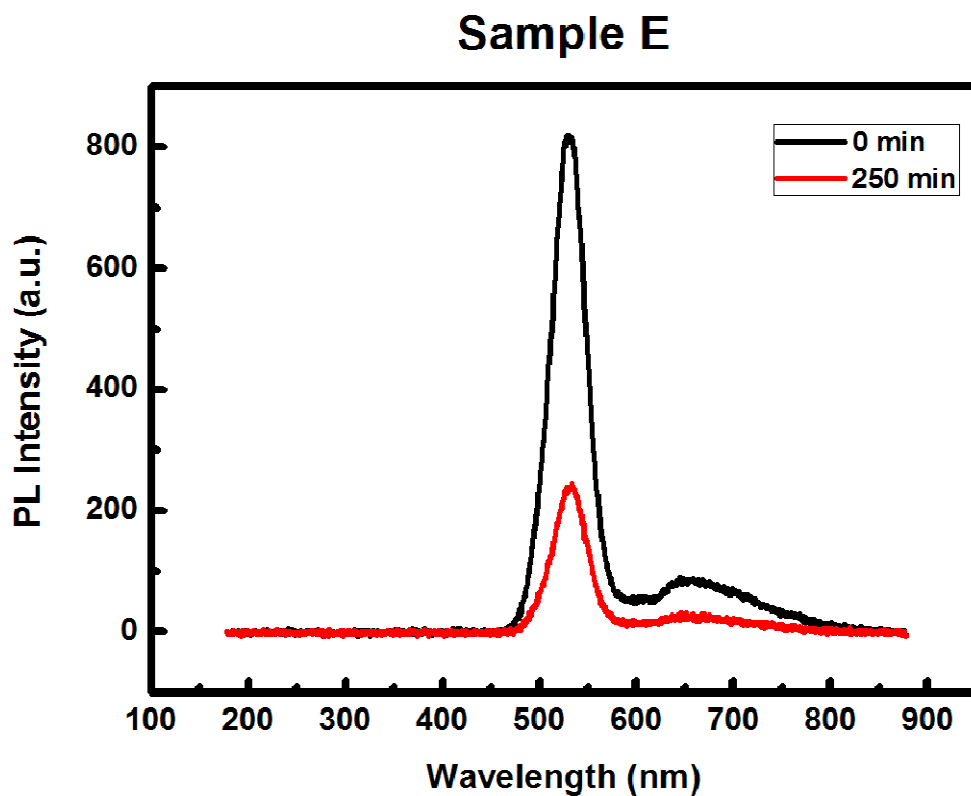


Fig. 4-11 PL spectrum in different excitation times of sample E.

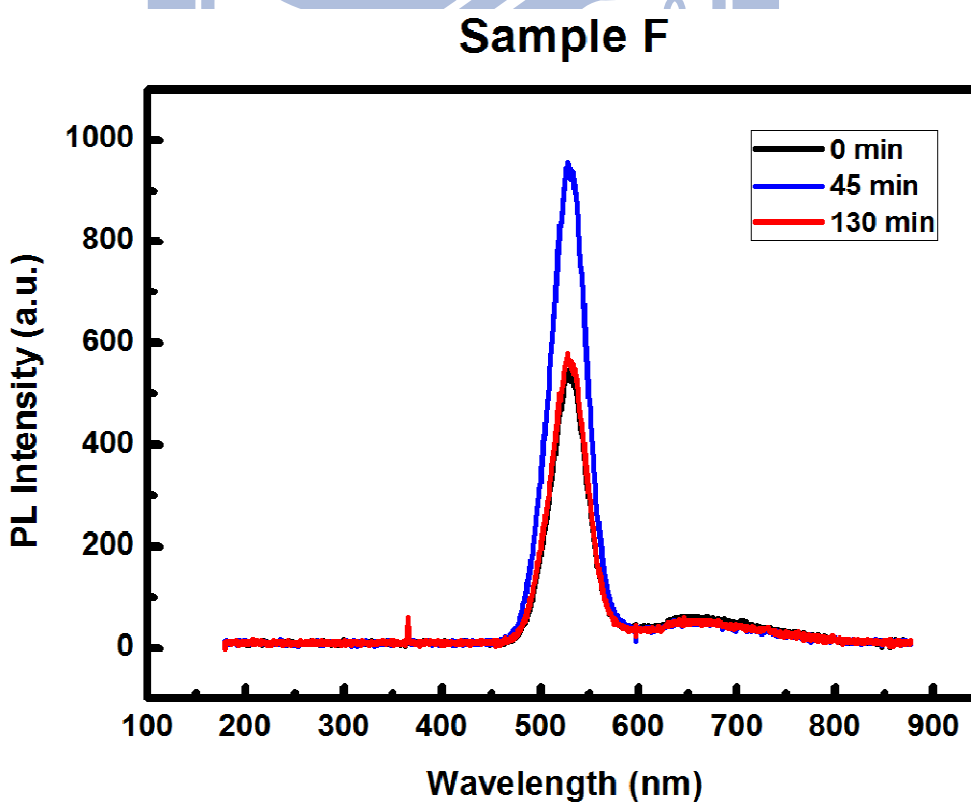


Fig. 4-12 PL spectrum in different excitation times of sample F.

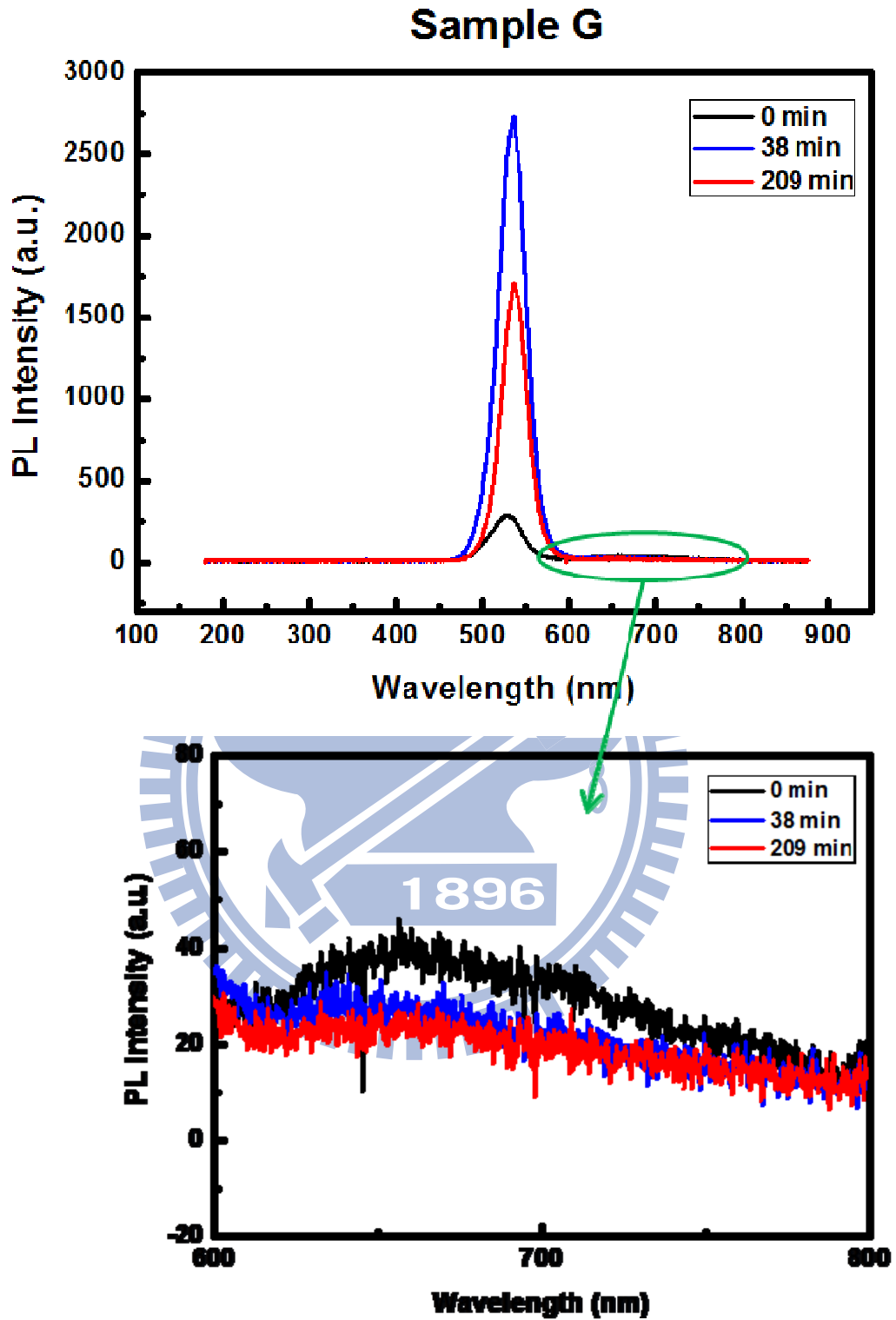


Fig. 4-13 PL spectrum in different excitation times of sample G.

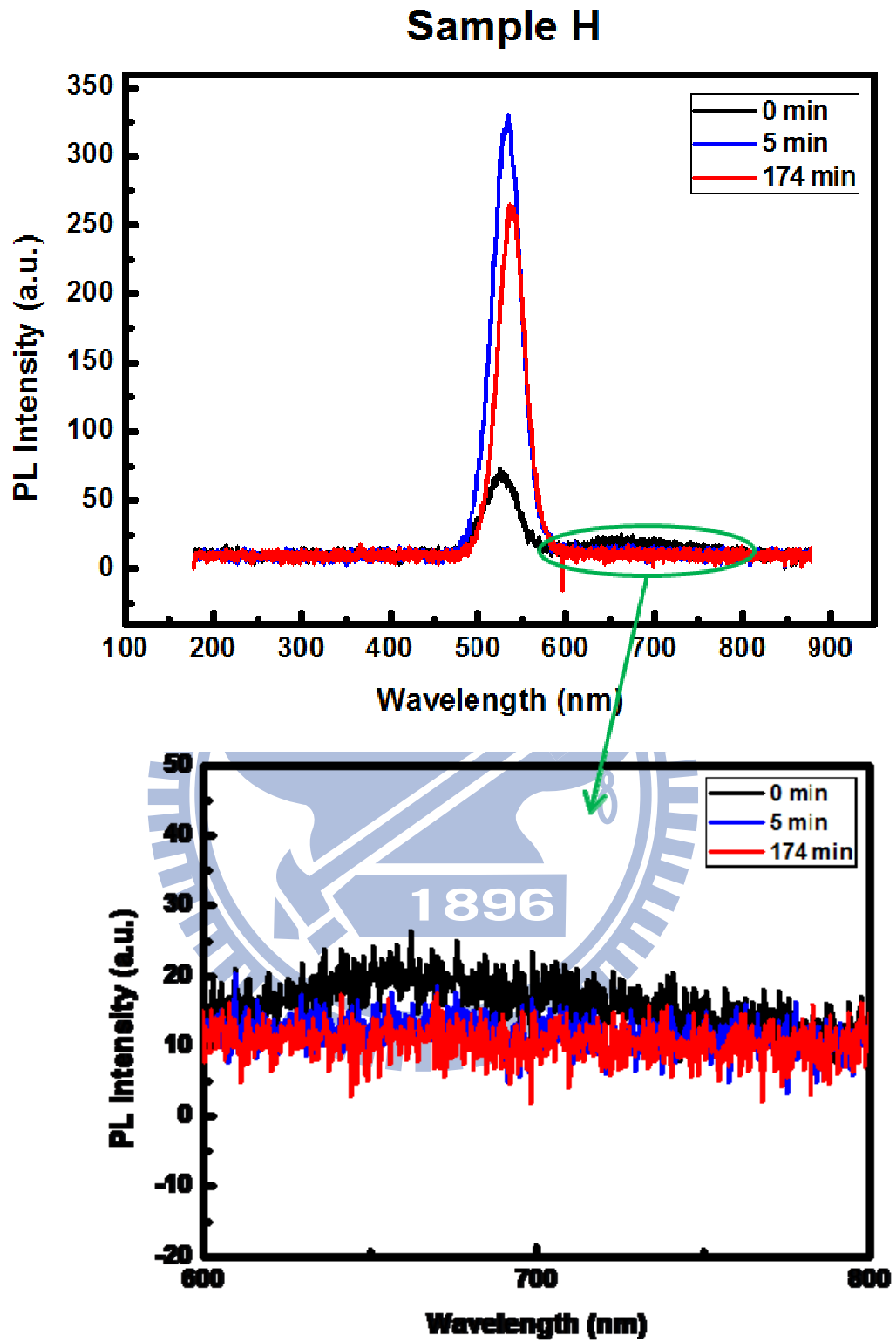


Fig. 4-14 PL spectrum in different excitation times of sample H.

In order to confirm that photoactivation effect can indeed reduce the surface defect, we compared the PL spectrum at different excitation times of each samples. In Fig. 4-12, 4-13, and 4-14, the defect-induced PL peak has decreased with the increase of excitation time.

Furthermore, we also used time-resolved PL (TR-PL) of sample G and H to measure the time constant and understand the recombination process of carriers and plotted in Fig. 4-15. The decay time constants of TR-PL signals are obtained from the fitting to the experimental data with the double exponential functions.



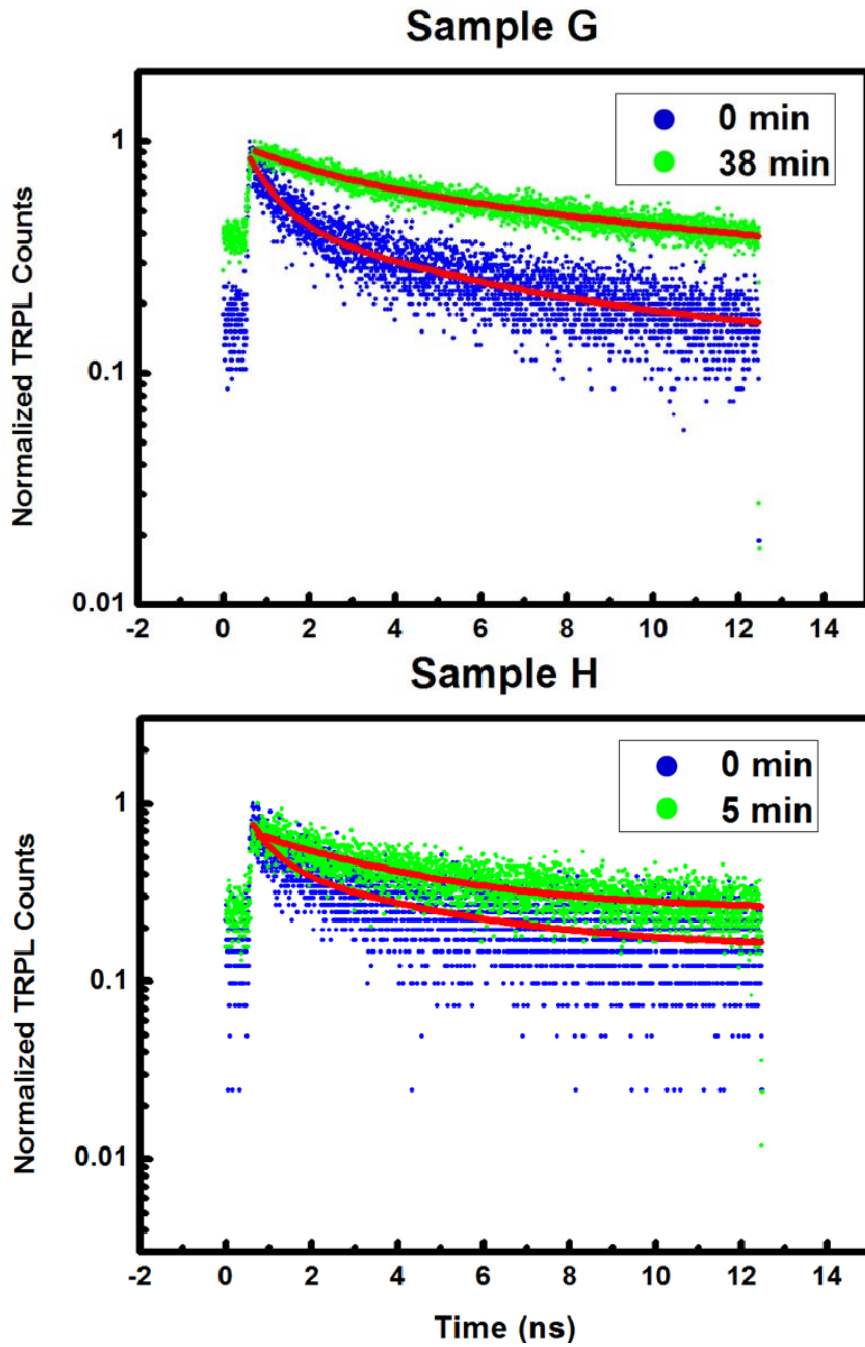


Fig. 4-15 Time-resolved photoluminescence curve of sample G,H.

	Excitation time	τ_1	τ_2
Sample G	0 min	5.38591	0.68674
	38 min	4.81212	
Sample H	0 min	3.74298	0.54484
	5 min	3.53771	

Table. 4-1 Time constant of sample G,H

In Table. 4-1, we show the time constant of sample G and H obtained at two different excitation times corresponding to the time at the highest PL peak. Sample G and H have one thing in common, which is when the PL peak is the highest, PL signal has only one time constant. This may be due to that after the completion of the photoactivation, the surface defects of CdSe nanoparticles have been replaced by SeO₂ layer and the carriers have only one recombination channel. This can confirm that the photoactivation actually can reduce the surface defect and enhance the PL intensity.

Moreover, Ref. 40 showed that mention the wavelength of laser and photon energy plays an important role in photoactivation. So we change the wavelength of laser from 365 nm to 400 nm, and repeated the same experiment to investigate the relation of wavelength and photoactivation.

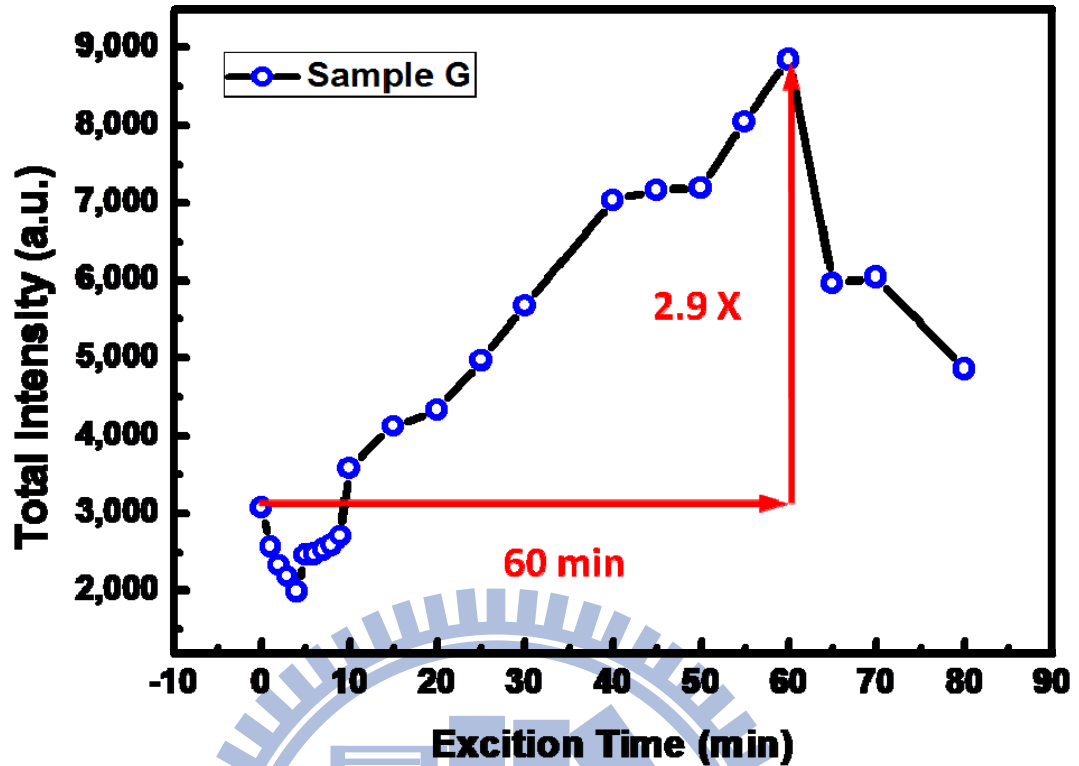


Fig. 4-16 Total PL intensity change with excitation time of sample G at 400 nm.

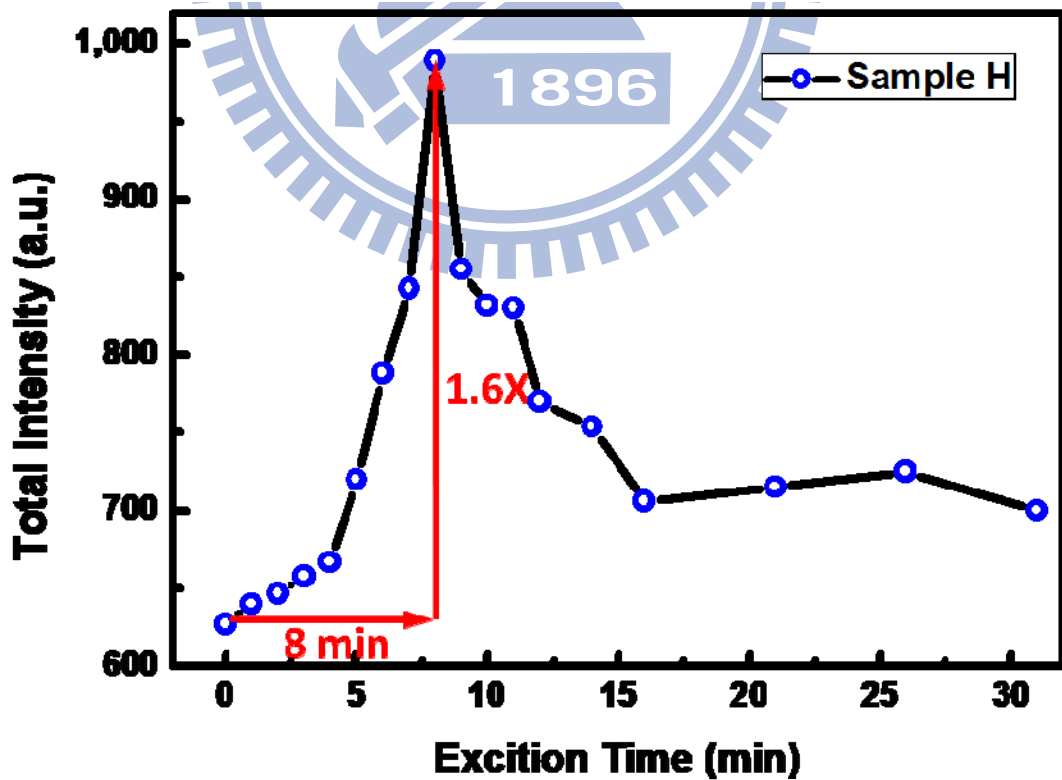


Fig. 4-17 Total PL intensity change with excitation time of sample H at 400 nm.

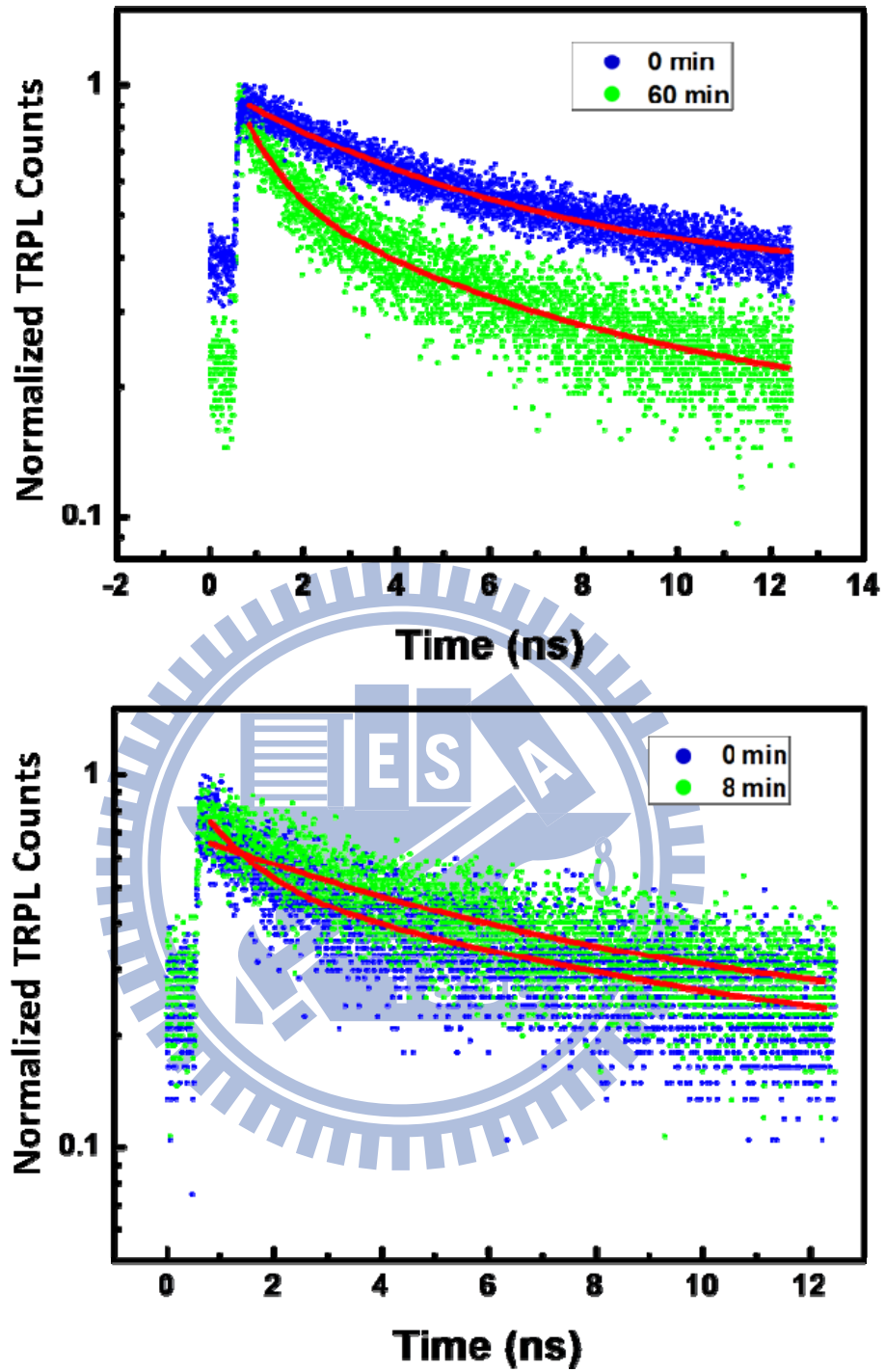


Fig. 4-18 Time-resolved photoluminescence curve of sample G,H.

	Excitation time	τ_1	τ_2
Sample G	0 min	5.43195	0.80586
	60 min	4.77284	
Sample H	0 min	8.57092	0.97587
	8 min	5.8104	

Table. 4-2 Time constant of sample G,H

Figure 4-16 and 4-17 show that when the wavelength of laser is changed from 365 nm to 400 nm, the photoactivation still exists and it reduces the surface defect. Compared to the results measured with 365 nm excitation laser pulses, the enhancement of PL intensity of the sample G and H is smaller and it takes longer time to reach the highest PL peak. It may be due to that the photon energy of 400 nm is smaller so that the absorbed energy transferred to the surface of nanoparticles becomes smaller. Then the production of SeO₂ layer becomes more difficult and results in the reduction of PL intensity enhancement and longer excitation time to the highest PL peak.

4.3 Z-scan System

4.3.1 Experiment Setup

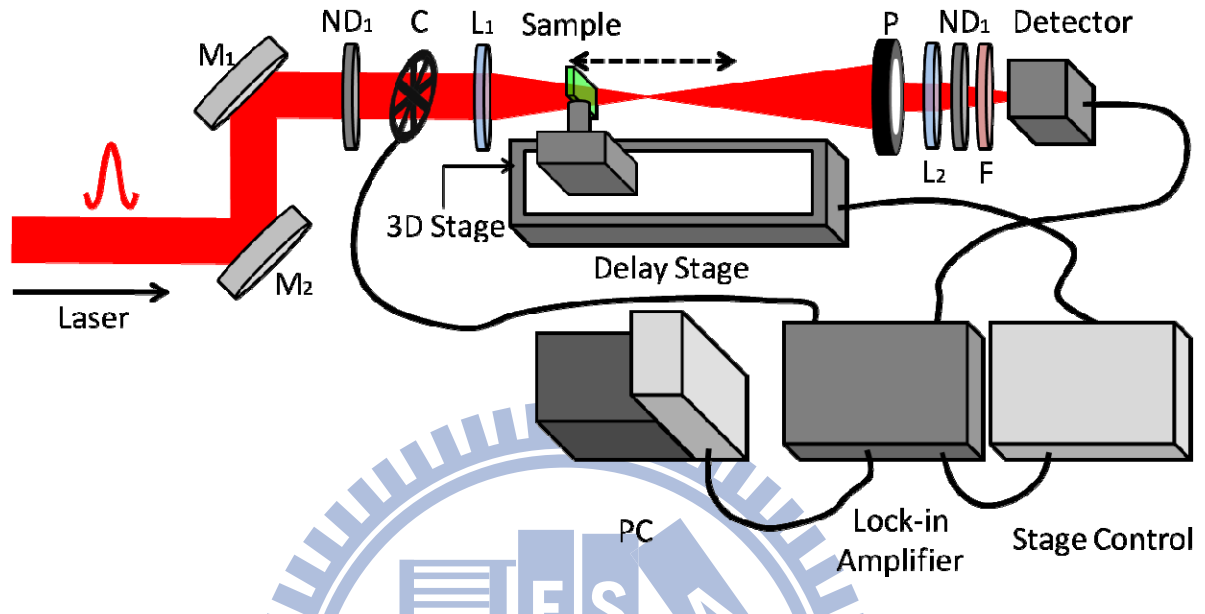


Fig. 4-19 Z-scan system setup

1. Laser : i. Ti:sapphire laser, wavelength: 800nm, max power: 400 mW, pulse width: 120 fs, repetition rate: 82 MHz.
ii. amplified, Ti:sapphire laser, wavelength: 800 nm, max power: 1.5 W, pulse width: 160 fs, repetition rate: 1 kHz.
2. M : silver mirror.
3. ND : ND Filter, ND₁ is used to adjust the incident laser power, ND₂ is used to prevent the saturation of detector.
4. C : chopper.
5. L : focusing lens.
6. P : pinhole.
7. F : edgepass filter, only let 800nm laser pass, block off the 520nm light emitted by CdSe.

The setup of the Z-scan system is shown in Fig. 4-19. A Ti:sapphire laser or an amplified Ti:sapphire laser is used to drive this system. A motorized translation stage is used to move sample from $+Z$ to $-Z$ with the spatial resolution of $10\ \mu\text{m}$. In order to increase the signal to noise ratio, an optical chopper and lock-in amplifier are used. In order to keep the thickness proper to measure Z-scan, a glass cell with the gap of $1\ \text{mm}$ was prepared to hold the liquid state of CdSe samples. (see Fig. 4-20) We chose the glass cell which is amorphous to prevent the occurrence of optical nonlinear effects by the focused intense laser pulses.

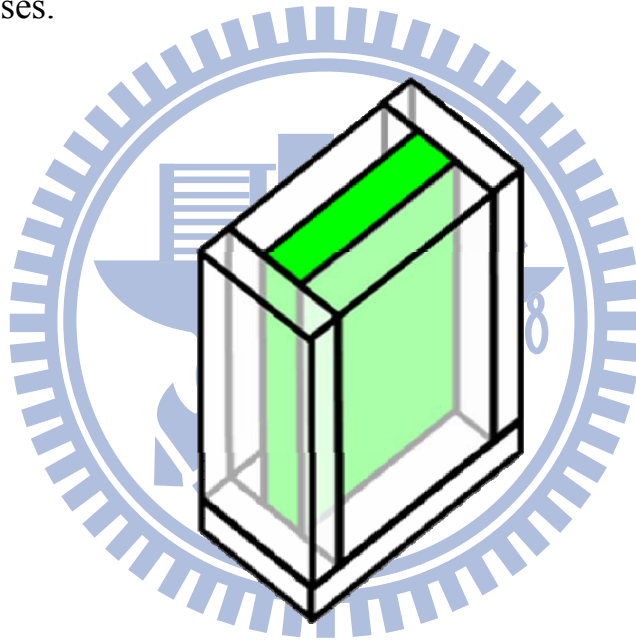


Fig. 4-20 Glass cell.

Prior to measure the CdSe sample, we measured the nonlinearity of ZnTe which has a large nonlinear coefficient and its value is already well known. Figure 4-21 shows the typical Z-scan trace of ZnTe and the nonlinear coefficients measured by our system. In our case, the two-photon absorption coefficient β we measured is 24.7 cm/GW, which is consistent with that of 16 cm/GW in the literature.^[43]

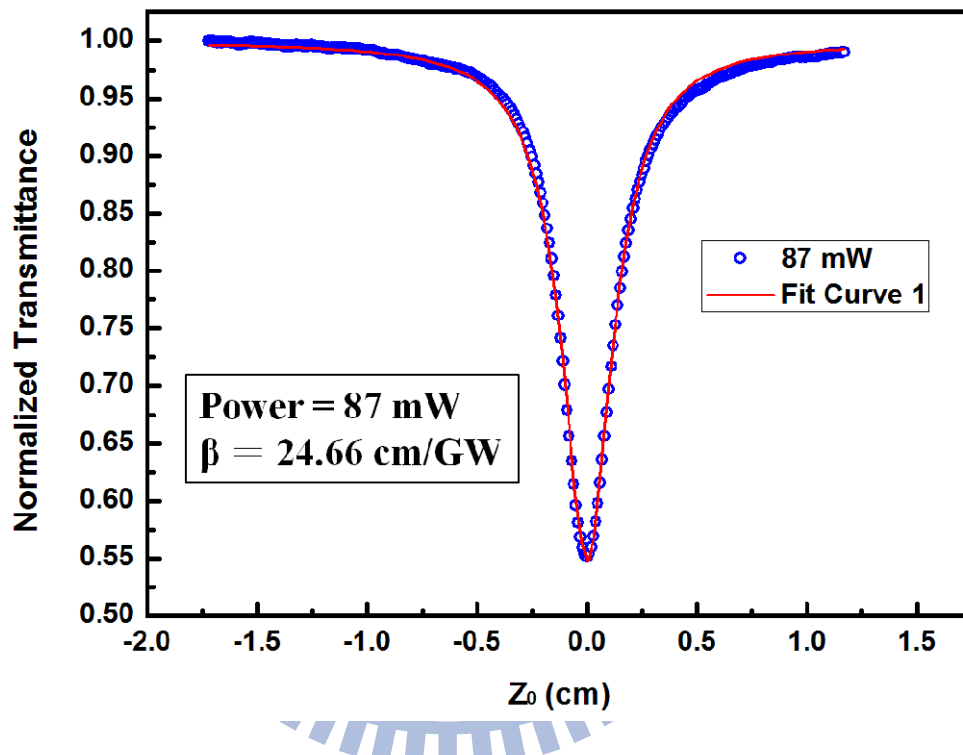


Fig. 4-21 Normalized transmittance with S=1 of ZnTe.

4.3.2 Result

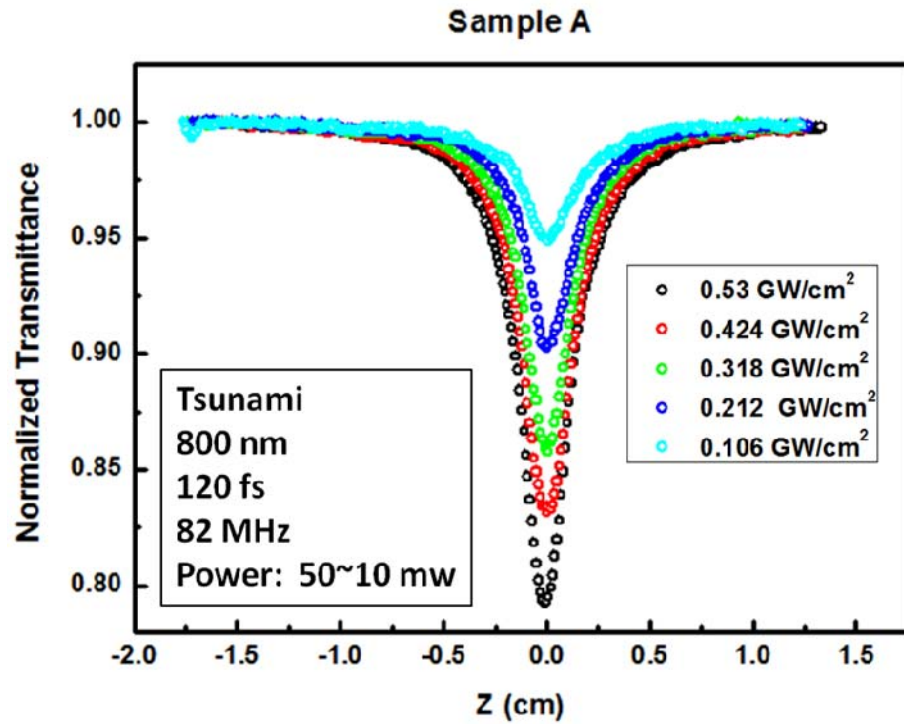


Fig. 4-22 Normalized transmittance with S=1 of sample A.

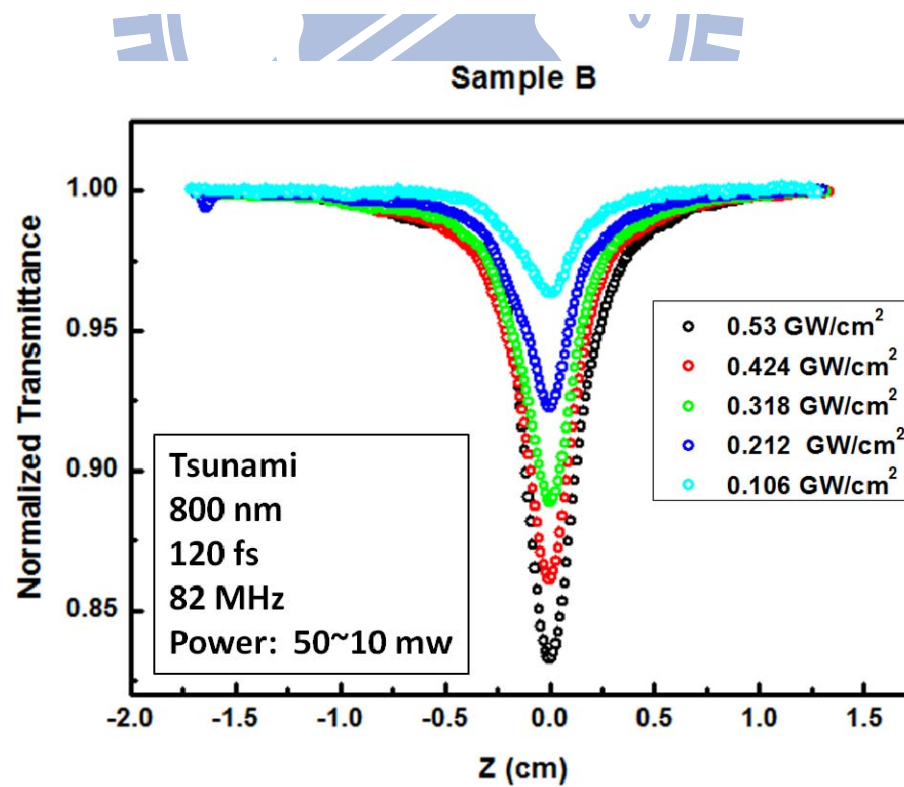


Fig. 4-23 Normalized transmittance with S=1 of sample B.

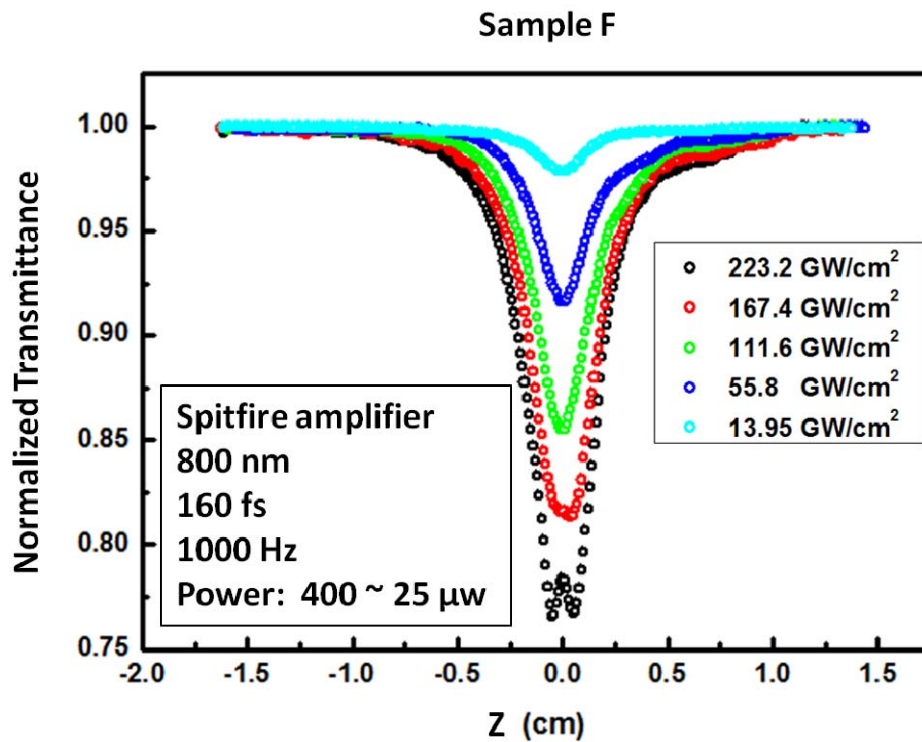


Fig. 4-24 Normalized transmittance with S=1 of sample F.

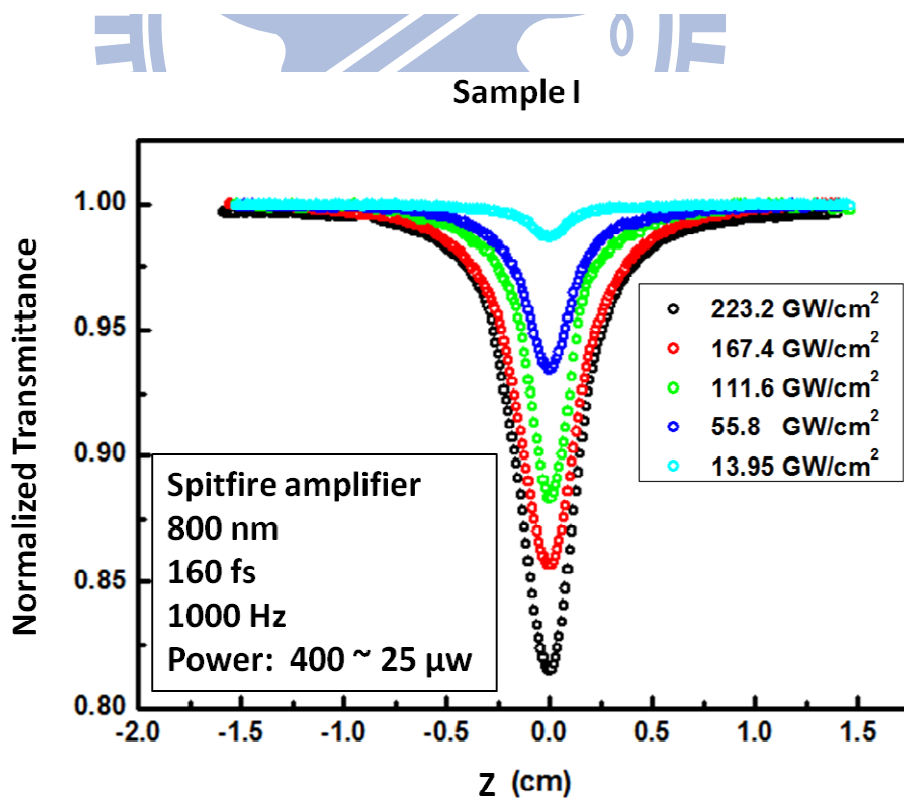
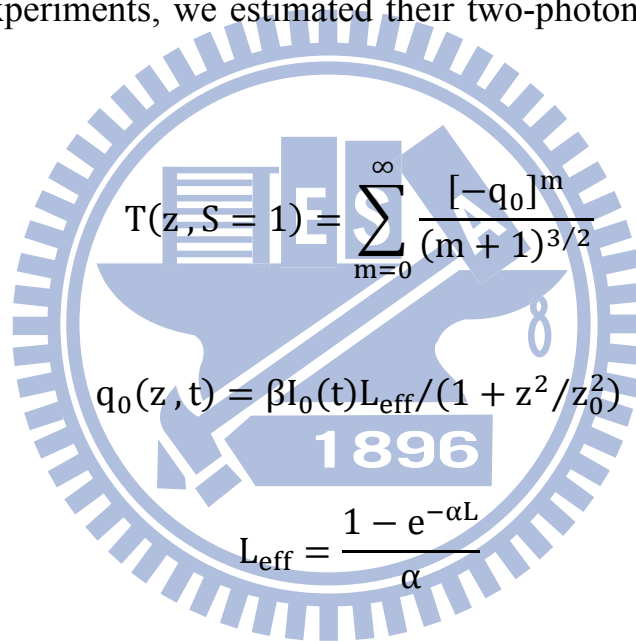


Fig. 4-25 Normalized transmittance with S=1 of sample I.

Figures 4-22 and 4-23 show the normalized transmittance signals from sample A and B, Cdse nanoparticles with tris-HCl and PBS as buffer, respectively, measured with the open aperture (S=1). Figure 4-24 and 4-25 are the Z-scan traces of sample F and I, CdSe nanoparticles with PVA with tris-HCl and PBS as buffer, respectively. Unamplified laser (Tsunami) was used as the light source for the measurement of sample A and B. Meanwhile the measurement of sample F and I was done with the amplified laser system (Spitfire) in order to get the measurable signal-to-noise ratio.

In these experiments, we estimated their two-photon absorption coefficient β by Eq. 2-18.



$$T(z, S = 1) = \sum_{m=0}^{\infty} \frac{[-q_0]^m}{(m + 1)^{3/2}}$$

$$q_0(z, t) = \beta I_0(t) L_{\text{eff}} / (1 + z^2/z_0^2)$$

$$L_{\text{eff}} = \frac{1 - e^{-\alpha L}}{\alpha}$$

First, we measure the absorption of sample A and B by UV/Vis absorption spectrometer. In the Fig. 4-26, the absorption of samples with Tris or PBS as buffer at 800 nm is 0. So, the L_{eff} is equal to the thickness of cell 0.1 cm.

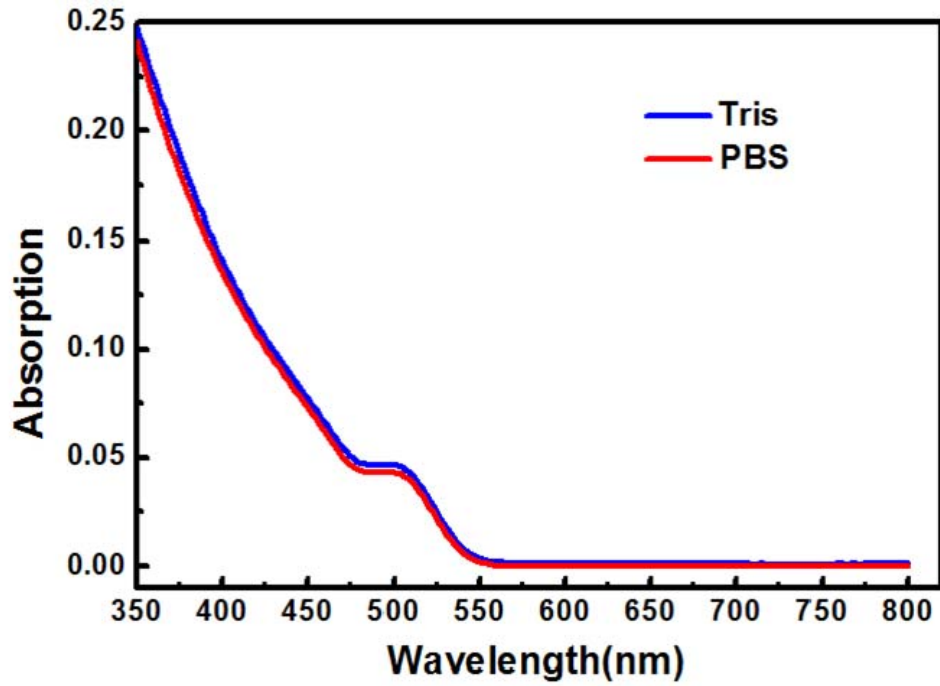


Fig. 4-26 Absorption of each samples.

Tsunami			Spitfire amplifier		
Power of Laser	Sample A	Sample B	Power of Laser	Sample F	Sample I
50 mW	15.9302	12.116	400 μ W	0.049	0.0328
40 mW	16.0967	12.7239	300 μ W	0.047	0.0334
30 mW	16.1667	12.7293	200 μ W	0.0469	0.0315
20 mW	15.8594	12.3866	100 μ W	0.0488	0.0357
10 mW	16.5155	12.4694	10 μ W	0.0464	0.0293
Average	16.1137	12.485		0.04762	0.03254

Table. 4-3 β (cm/GW) of each samples.

sample A. Therefore, the probability of two photon absorption becomes smaller in sample B and results in the smaller two photon absorption coefficient β . In the second part, the two photon absorption coefficients β of sample F and sample I are close. Because when we add PVA, the CdSe nanoparticles are capped by PVA to form a PVA cluster. They have similar structure, so the two photon absorption coefficients β are close.

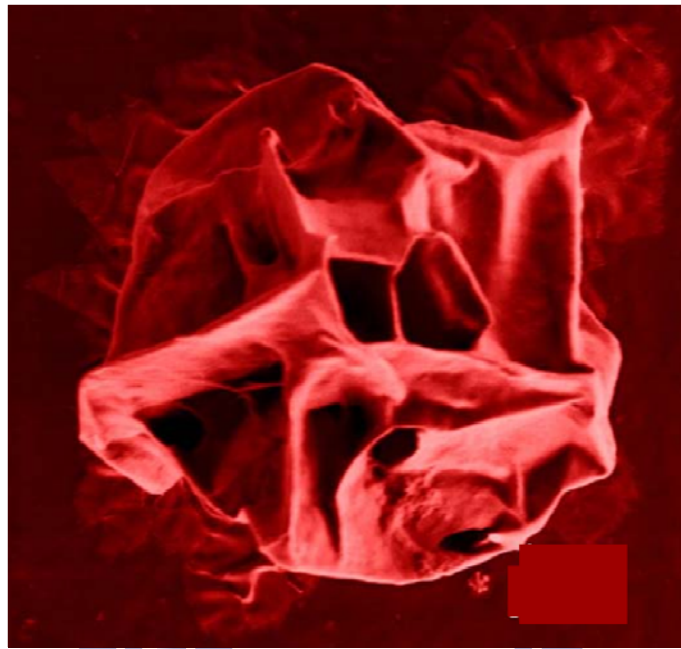


Fig. 4-28 The CdSe nanoparticles/PVA cluster.

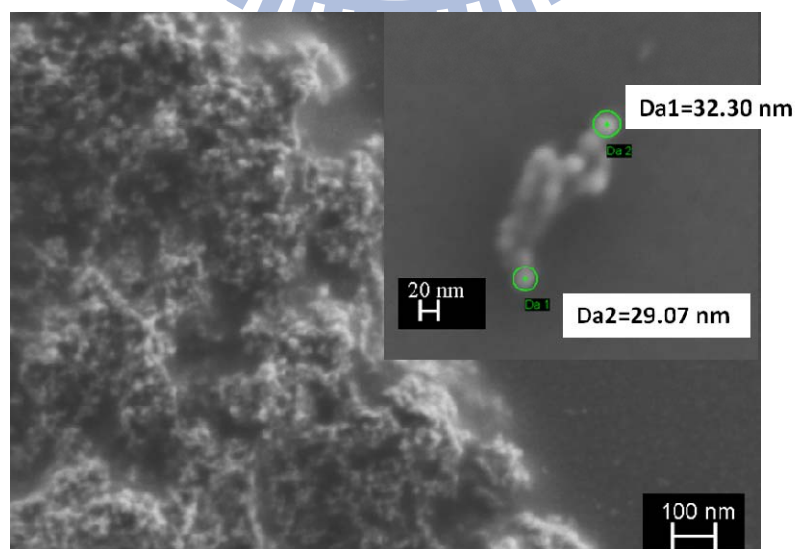


Fig. 4-29 FESEM imaging of sample F

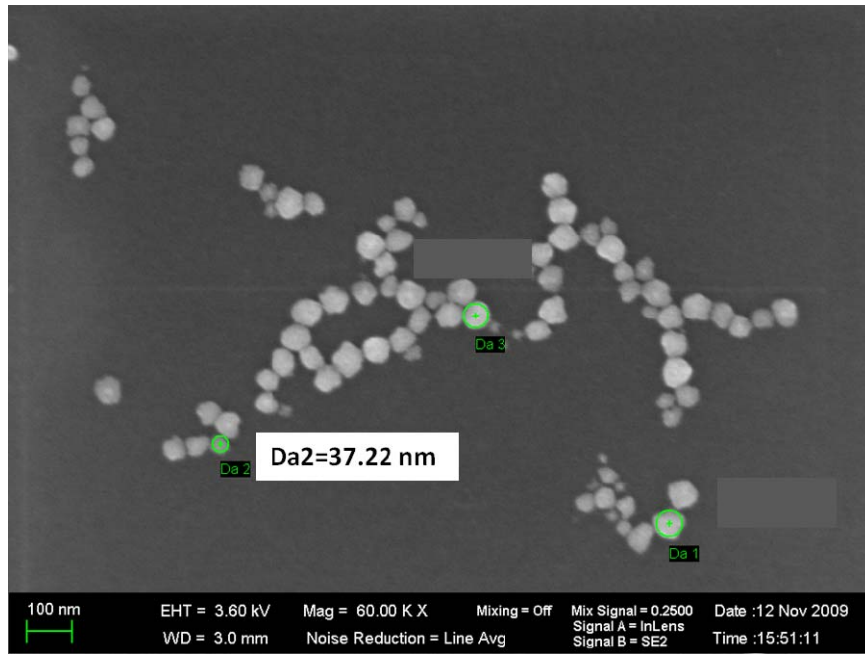


Fig. 4-30 FESEM imaging of sample I



Chapter5 Conclusion

In this thesis, we have investigated the photoluminescence and optical nonlinearity of water-soluble PVA-capped CdSe nanoparticles. The experiment could be summarized to two parts: 1. photoactivation 2. two photon absorption coefficient β .

(1) Photoactivation

We found the photoactivation occurs during the exposure by ultrafast laser. Upon irradiation, the PL intensity linearly increases with the increase of the excitation time and the surface defect can be reduced. The reaction involving the PL activation is dependent on the wavelength of the irradiated light. Larger photon energy excitation induces a relatively good photoactivation effect. In addition, the CdSe/PVA ratio also can influence the photoactivation. Sample G with the CdSe/PVA ratio of 1/10 shows the highest PL intensity enhancement and photoactivation effect.

(2) Two photon absorption coefficient β

We measured the two photon absorption coefficient β of CdSe nanoparticle with different buffers. We found that number of CdSe nanoparticles in a unit area influence β . When the number of nanoparticles in a unit area becomes small, accordingly the probability of light absorption is reduced and reduces the β .

Reference

- [1] Andrew M. Smith , Shuming Nie , “Semiconductor Nanocrystals: Structure, Properties, and Band Gap Engineering” , *Accounts of chemical research* , Vol. 43 , pp.190-200 , 2010
- [2] Genoveva Zlateva , Zhivko Zhelev , Rumiana Bakalova and Iwao Kanno , “Precise Size Control and Synchronized Synthesis of Six Colors of CdSeQuantum Dots in a Slow-Increasing Temperature Gradient” , *Inorg. Chem.* , Vol.46 , pp.6212-6214 , 2007
- [3] Manoj Nirmal , Louis Brus , “Luminescence Photophysics in Semiconductor Nanocrystals” , *Acc. Chem. Res.* , Vol. 32 , pp.407-414 , 1999
- [4] Louis Brus , “Electronic Wave Functions in Semiconductor Clusters: Experiment and Theory” , *J. Phys. Chem.* , Vol. 90 , pp.2555-2560 , 1986
- [5] Hiroyuki Tetsuka , Takeo Ebina and Fujio Mizukami , “Highly Luminescent Flexible Quantum Dot–Clay Films ” , *Adv. Mater.* , Vol. 20 , pp.3039–3043 , 2008
- [6] C. B. Murray , D. J. Noms and M. G. Bawendi , “Synthesis and Characterization of Nearly Monodisperse CdE(E = S, Se, Te) Semiconductor Nanocrystallites” , *J. Am. Chem. Soc.* , Vol.115 , pp. 8706-8715 , 1993
- [7] D. J. Noms , C. B. Murray and M. G. Bawendi , “Measurement of the Size Dependent Hole Spectrum in CdSe Quantum Dots” , *Physical Review Letters.* , Vol. 72 , pp. 2612-2615 , 1994
- [8] Dmitri V. Talapin , Andrey L. Rogach , Andreas Kornowski , Markus Haase and Horst Weller , “Highly Luminescent Monodisperse CdSe and CdSe/ZnS

- Nanocrystals Synthesized in a Hexadecylamine-Trioctylphosphine Oxide-Trioctylphosphine Mixture” , *Nano Letters* , Vol. 1 , No. 4 , pp.207-211 , 2001
- [9] Gregory Kalyuzhny , Royce W. Murray , “Ligand Effects on Optical Properties of CdSe Nanocrystals “ , *J. Phys. Chem. B* , Vol.109 , pp.7012-7021 ,2005
- [10]Jose Aldana , Y. Andrew Wang , Xiaogang Peng , “Photochemical Instability of CdSe Nanocrystals Coated by Hydrophilic Thiols” , *J. Am. Chem. Soc.* , Vol.123 , pp.8844-8850 , 2001
- [11]Xiaobo Chen , Yongbing Lou , Anna C. Samia and Clemens Burda , “Coherency Strain Effects on the Optical Response of Core/Shell Heteronanostructures” , *NANO LETTERS*, Vol. 3 , No. 6 , pp.799-803 , 2003
- [12]J. Jack Li , Y. Andrew Wang , Wenzhuo Guo , Joel C. Keay , Tetsuya D. Mishima , Matthew B. Johnson , and Xiaogang Peng , “Large-Scale Synthesis of Nearly Monodisperse CdSe/CdS Core/Shell Nanocrystals Using Air-Stable Reagents via Successive Ion Layer Adsorption and Reaction” , *J. AM. CHEM. SOC.* , Vol.125 , pp.12567-12575 , 2003
- [13]P. Reiss a , S. Carayon b , J. Bleuse b , A. PronLow , ”polydispersity core/shell nanocrystals of CdSe/ZnSe and CdSe/ZnSe/ZnS type: preparation and optical studies” , *Synthetic Metals* , Vol.139 , pp.649–652 , 2003
- [14]A. Mews , A. Eychmiiller , M. Giersig , D. Schooss , H. Weller , “Preparation, Characterization, and Photophysics of the Quantum Dot Quantum Well System CdS/HgS/CdS” , *J. Phys. Chem.* , Vol.98 , pp.934-941 , 1994
- [15]Margaret A. Hines , Philippe Guyot-Sionnest , “Synthesis and

- Characterization of Strongly Luminescing ZnS-Capped CdSe Nanocrystals” , *J. Phys. Chem.* , Vol.100 , pp.468-4711 , 1996
- [16]Warren C. W. Chan , Shuming Nie , “Quantum Dot Bioconjugates for Ultrasensitive Nonisotopic Detection” , *Science* , Vol.281, pp.2016 , 1998
- [17]Z. Adam Peng , Xiaogang Peng , “Mechanisms of the Shape Evolution of CdSe Nanocrystals” , *J. Am. Chem. Soc.* , Vol.123 , pp.1389-13951 , 2001
- [18]Lingjie Guo , Peter R. Krauss , Stephen Y. Chou , “Nanoscale silicon field effect transistors fabricated using imprint lithography” , *Appl. Phys. Lett.* , Vol. 71 , No. 13 , pp.1881-1883 , 1997
- [19]Xiaogang Peng , Michael C. Schlamp , Andreas V. Kadavanich , A. P. Alivisatos , “Epitaxial Growth of Highly Luminescent CdSe/CdS Core/Shell Nanocrystals with Photostability and Electronic Accessibility” , *J. Am. Chem. Soc.* , Vol.119 , pp. 7019-70291 , 1997
- [20]B. O. Dabbousi , J. Rodriguez-Viejo , F. V. Mikulec , J. R. Heine , H. Mattoussi , R. Ober , K. F. Jensen , M. G. Bawendi , “(CdSe)ZnS Core-Shell Quantum Dots: Synthesis and Characterization of a Size Series of Highly Luminescent Nanocrystallites” , *J. Phys. Chem. B* , Vol.101 , pp.9463-94751 , 1997
- [21]Sungjee Kim , Brent Fisher , Hans-Jurgen Eisler , Mounji Bawendi , “Type-II Quantum Dots: CdTe/CdSe(Core/Shell) and CdSe/ZnTe(Core/Shell)” , *J. AM. CHEM. SOC.* , Vol.125 , pp.11466-114671 , 2003
- [22]K. L. Chopra , P. D. Paulson , V. Dutta , “Thin-Film Solar Cells: An Overview” , *Res. Appl.* , Vol. 12 , pp.69–92 , 2004

- [23]Chin-Yi Liu , Zachary C. Holman , Uwe R. Kortshagen , “Hybrid Solar Cells from P3HT and Silicon Nanocrystals” , *Nano Lett.* , Vol. 9 , No. 1 , pp.449-452 , 2009
- [24]Istva’n Robel , Bruce A. Bunker , Prashant V. Kamat , Masaru Kuno , “Exciton Recombination Dynamics in CdSe Nanowires: Bimolecular to Three-Carrier Auger Kinetics” , *Nano Lett.* , Vol. 6 , No. 7 , pp.1344-1349 , 2006
- [25]C. Simbrunner , G. Hernandez-Sosa , E. Baumgartner , G. Hesser , J. Roither, W. Heiss , H. Sitter , “Para-sexiphenyl-CdSe/ZnS nanocrystal hybrid light emitting diodes” , *Appl. Phys. Lett.* , Vol.94 , pp.073505 , 2009
- [26]Wonkeun Chung , Kwanhwi Park , Hong Jeong Yu , Jihyun Kim , Byung-Hee Chun , Sung Hyun Kim , “White emission using mixtures of CdSe quantum dots and PMMA as a phosphor” , *Optical Materials* , Vol.32 , pp.515–521 , 2010
- [27]Weibo Cai , Dong-Woon Shin , Kai Chen , Olivier Gheysens , Qizhen Cao , Shan X. Wang , Sanjiv S. Gambhir , Xiaoyuan Chen , “Peptide-Labeled Near-Infrared Quantum Dots for Imaging Tumor Vasculature in Living Subjects” , *Nano Lett.* , Vol. 6 , No. 4 , pp.669-676 , 2006
- [28]Yan Lai , Ying Yu , Ping Zhong , Jianzhong Wu , “Development of Novel Quantum Dots as Fluorescent Sensors for Application in Highly Sensitive Spectrofluorimetric Determination of Cu^{2+} ” , *Analytical Letters* , Vol.39 , pp.1201–1209 , 2006
- [29]Jia-Min Shieh , Yi-Fan Lai , Yong-Chang Lin , Jr-Yau Fang , “Photoluminescence: Principles, Structure, and Applications” , 奈米通訊 , 第十二卷第二期

- [30] Timothy H. Gfroerer , "Photoluminescence in Analysis of Surfaces and Interfaces" , Encyclopedia of Analytical Chemistry.
- [31] G.D. Gilliland , "Photoluminescence spectroscopy of crystalline semiconductors" , Materials Science and Engineering: R: Reports , Vol.18 , Issues 3-6 , pp.99-399 , 1997
- [32] M. Sheik-Bahae , A. A. Said , E. W Van Stryland , "High sensitivity, single-beam n_2 measurement" , Opt. Lett. , Vol.14 , 955 , 1989
- [33] MANSOOR SHEIK-BAHAE , MEMBER, IEEE, ALI A. SAID , TAI-HUEI WEI , DAVID J. HAGAN , MEMBER, IEEE AND E. W. VAN STRYLAND , SENIOR MEMBER, IEEE , "Sensitive Measurement of Optical Nonlinearities Using a Single Beamz" , *IEEE* , VOL. 26 , NO. 4 , 1990
- [34] A. A. Said , M. Sheik-Bahae , D. J. Hagan , T. H. Wei , J. Wang , J. Young , E. W. Van Stryland , "Determination of bound-electronic and free-carrier nonlinearities in ZnSe, GaAs, CdTe, and ZnTe" , *Optical Society of America* , Vol. 9 , No. 3 , pp.405-414 , 1992
- [35] D. A. B. Miller , S. D. Smith , A. M. Johnston , "Optical bistability and signal amplification in a semiconductor crystal: applications of new low power effects in InSb" , *App. Phys. Lett.* , Vol.35, 1979
- [36] H. M. Gibbs , S. L. McCall , T. N. Venkatesan , A. C. Gossard , A. Passner , W Wiegmann , "Optical bistability in semiconductors" , *Appl. Phys. Lett.* , Vol.35 , 1979.
- [37] A. Miller , D. Duncan , "Optical nonlinearities in narrowgap semiconductors" , *Optical Properties of Narrow-Gap Low-Dimensional Structures*
- [38] 黃東慶 , 「高亮度硒化鎘/聚乙醇固態複合式材料之合成與鑑定」, 國

立中興大學，碩士論文，民國 99 年。

- [39]Shu-Juan Fu , Tung-Ching Huang , Ching-Yuan Cheng , Hyeyoung Ahn , Sheng-Yueh Changd and Kuan-Jiuh Lin , “Direct access to green-emissive CdSe quantum nanoclusters in sphere-like monoliths and their use as LED phosphors” , not been published yet.
- [40]Carolina Carrillo-Carrión , Soledad Cárdenas , Bartolomé M. Simonet and Miguel Valcá rcel , “Quantum dots luminescence enhancement due to illumination with UV/Vis light” , *Chem. Commun.* , pp.5214–5226 , 2009
- [41]S. R. Cordero , P. J. Carson , R. A. Estabrook , G. F. Strouse , and S. K. Buratto , “Photo-Activated Luminescence of CdSe Quantum Dot Monolayers” , *J. Phys. Chem. B* , Vol. 104 , pp.12137-12142 , 2000
- [42]Chaoqing Dong , Huifeng Qian , Nenghu Fang , and Jicun Ren , “On-Line Investigation of Laser-Induced Aggregation and Photoactivation of CdTe Quantum Dots by Fluorescence Correlation Spectroscopy ” , *J. Phys. Chem. C* , Vol. 111 , pp.7918-7923 , 2007
- [43]王蒼祺，「Z-掃描量測碲化鋅之三階非線性效應」，國立交通大學，碩士論文，民國 90 年。
- [44]H. H. Huang , F. Q. Yan , Y. M. Kek , C. H. Chew , G. Q. Xu , W. Ji , P. S. Oh , and S. H. Tang , “Synthesis, Characterization, and Nonlinear Optical Properties of Copper Nanoparticles” , *Langmuir* , Vol. 13 , pp. 172-175 , 1997